Vortex Ring State in Multi-Rotor Aircraft: Boundary Estimations and their Uncertainty

A Ring Vortex Model Approach Applied to the CH-47 Chinook

MSc Thesis

Xander Bonenkamp



TU Delft

Vortex Ring State in Multi-Rotor Aircraft: Boundary Estimations and their Uncertainty

A Ring Vortex Model Approach Applied to the CH-47 Chinook

Thesis report

by

Xander Bonenkamp

to obtain the degree of Master of Science
at Delft University of Technology,
to be publicly defended on 22 September at 11:00.

Thesis committee:

Chair:	Dr. S. Theodoulis
Responsible supervisor:	Prof. M.D. Pavel
External examiner:	Dr. A. Bombelli
RNLASF supervisor:	Capt. Steven
Place:	Faculty of Aerospace Engineering Delft University of Technology
Project duration:	December 2025 - September 2026
Student number:	5491770

An electronic version of this thesis is available at `https://repository.tudelft.nl/`.

Cover: Royal Netherlands Air and Space Force (RNLASF) CH-47F Chinook. Cover photograph used with the photographer's permission. © Ludo Mennes, Northern Skies Aviation.

TU Delft

RNLAF FLIGHT TEST

Summary

The vortex ring state (VRS) is an aerodynamic phenomenon in which a rotor in descent can experience a sudden increase in rate of descent, uncommanded pitching and rolling, and reduced control-effectiveness. Close to the ground, VRS can be a dangerous phenomenon. Many helicopter accidents have been attributed to VRS, showing the need for the phenomenon to be understood, specifically its entry conditions. The VRS boundaries of the CH-47 Chinook are not well documented in open literature. The Chinook is a tandem-rotor helicopter, where the front and aft rotors partially overlap or intersect, and therefore show aerodynamic interference. Not only does the presence of a second rotor influence the inflow through the other rotor. The neighboring rotor intermeshes with the other rotor and is envisioned to sweep right through the existing vortex structure, which is predominant in VRS.

The purpose of this thesis was to investigate whether a low-fidelity model of rotors and their wake in descent can be used to predict VRS boundaries for both single- and tandem-rotor configurations. Low-fidelity models are simpler, often use experimental data, and the topology of the modeled wake is prescribed, if modeled at all. The ring vortex model (RVM) was selected, and extended to model overlapping rotors. RVM is a low-fidelity simulation approach that approximates the vortex structure of the wake as a series of vortex rings with a diameter equal to that of the rotor. They move along the wake with the local velocity, and can not deform, break, tilt, or grow in strength. As it has a lower computational cost than mid- or high-fidelity models, RVM was selected because the model had to be evaluated repeatedly for an uncertainty quantification (UQ). RVM was coupled to an augmentation of the Pitt-Peters inflow model and blade element theory. This augmentation mitigated the non-physical discontinuity between the helicopter- and windmill-branches predicted by momentum theory for a rotor in descent. The bifurcation criterion was used to determine the VRS boundaries by identifying the reversal in the gradient of the trim curve. VRS was marked by an increasing rate of descent beginning to require an increase, rather than a decrease, in collective pitch to maintain trim. For the tandem-rotor, the effect of each wake on both rotors was included, but wake-wake interference was not.

The deterministic single-rotor results were found to be in agreement with experimental flight-test data from the *Office National d'Études et de Recherches Aérospatiales* (ONERA) and European Union Aviation Safety Agency (EASA) for lower forward speeds. For higher forward speeds, the model was not in agreement with experimental data. For the tandem-rotor, the data showed that interference between rotors affects the predicted VRS boundary. In axial descent, both rotors were more prone to VRS compared to an identical but isolated single rotor. In oblique descent, the front rotor showed a smaller range of rates of descent at which VRS can occur. Furthermore, VRS ceased to occur at lower forward speeds. For the aft rotor, VRS was encountered at a larger range of rates of descent and at higher forward speeds too. This asymmetry could result in uncommanded pitching of the Chinook in VRS. Unfortunately, no experimental data was available for the Chinook to validate these results.

A UQ was performed using Latin hypercube sampling (LHS) and polynomial chaos expansion (PCE). The bounds of VRS showed significant uncertainty using LHS. This was caused by the uncertainties in experimental data used in RVM, and the RVM's inability to accurately model the wake in VRS. For the tandem rotors, the uncertainty of the VRS boundaries was found to be smaller than that of the single rotors. However, the uncertainty varied more over the range of forward speeds, with different uncertain parameters being dominant. PCE was applied in an attempt to reduce the computational cost of the UQ. It creates a pseudo-model using orthogonal polynomials allowing for a computationally cheap method to acquire more samples. However, PCE was deemed unfit for this VRS model, and may also be unsuitable for other VRS models.

The main recommendation for further research is to employ a mid-fidelity model, as RVM (a low-fidelity model) has various severe limitations that are inherent to the model. Furthermore, (additional) experimental data for a conventional single rotor helicopter, and especially the Chinook, is strongly desired to validate the findings of this and further research.

Preface

In order to obtain my Master's degree from TU Delft, I was required to write a thesis. Having developed a special interest in helicopters during my Bachelor's, I hoped to conduct my thesis research on this topic. After a meeting with Marilena, she proposed VRS as a research topic and agreed to supervise my thesis. In October 2025, I was still at my internship at the RNLASF in Utrecht. I greatly enjoyed this internship under the supervision of Wilbert and Hielke, and after discussing my upcoming thesis there, the opportunity arose to conduct my thesis at the RNLASF. I would be placed within the rotary-wing branch of KTV at Gilze-Rijen.

From KTV, I would particularly like to thank Steven for his guidance, proactive support in arranging practical matters, and good company throughout my thesis. His feedback was always constructive and very useful, and I believe his guidance greatly improved this report. I would also like to thank him for showing me around the organization. I greatly enjoyed flying in the Chinook simulator, sitting in the cockpit of a Chinook, and visiting ETPS in England. These were truly unique and exciting experiences that I do not think are available during many internships. Thank you, Steven! I would also like to thank Theo and Patrick for finding and arranging this thesis opportunity. Without them, I would not have been able to conduct my thesis at the RNLASF, something I had strongly hoped for. Furthermore, I would like to thank Arjan for the good company, and Joost for arranging the opportunity to see some F-35s, as well as for the entertaining stories over a drink after 5 p.m. I would like to thank Dushi for organizing the weekly sports sessions and for answering so many of my questions about being a military pilot. Finally, I would like to thank Bert for his excellent advice to 'go around the airfield and see cool things'. Standing so close to an airborne Chinook together with the MAOT was a unique experience. I greatly enjoyed my time at KTV, especially the get-togethers in the Squadron Bar and KTV couch corner at the end of the day, cycling together, and seeing and experiencing so much of the organization.

From Delft, I would like to thank my supervisor, Marilena. Her extensive knowledge of helicopter research was very valuable in guiding my research. I also enjoyed the conversations following our bi-weekly meetings, and I appreciate her interest in my progress through the Air Force pilot selection programme. I would also like to thank my friends in Delft: Ivo, Lauren, and Hubert. Meeting in Delft to work on our theses, including the sporting breaks in the form of swimming and running, really helped me through the more challenging parts of writing a thesis.

From Utrecht, I would like to thank my mom and dad for their support throughout my thesis and my studies in general. I especially appreciated their support during the busier months of my thesis. I would also like to thank my grandfather for his support throughout my studies, and my siblings Jasper, Maaike, and Tobias for their interest in my studies. Last but not least, I would like to thank Julia for her support and company during our study/thesis sessions together.

I learned a great deal during this thesis, particularly about conducting, organizing, and documenting research. These are valuable lessons that I will undoubtedly carry with me into my working life, which will begin with pilot training at the RNLASF, a long-cherished ambition.

Xander Bonenkamp
Gilze-Rijen, August 2026

Contents

Summary ii

Preface iv

Nomenclature ix

1 Introduction 1
- 1.1 Background and research objective . . . 1
- 1.2 Research Question . . . 2
- 1.3 Scope . . . 3
- 1.4 Outline . . . 3

2 Literature Review 4
- 2.1 Vortex Ring State . . . 4
- 2.2 Experimental Observations . . . 9
- 2.3 Modeling Approaches for VRS . . . 10
- 2.4 Inflow Modeling . . . 14
- 2.5 Rotor-Rotor Interference . . . 15
- 2.6 VRS boundary determination . . . 16
- 2.7 Uncertainty Quantification . . . 17
- 2.8 Summary and Knowledge Gap . . . 18

3 Methodology 19
- 3.1 Ring Vortex Model . . . 19
- 3.2 Inflow Model and Blade Element Theory . . . 21
- 3.3 VRS Boundaries Determination . . . 24
- 3.4 Tandem-Rotor Interference Model . . . 27
- 3.5 Assumptions . . . 30

4 Deterministic VRS boundaries 31
- 4.1 Single Rotor VRS Bound . . . 31
- 4.2 Tandem-Rotor VRS Bound . . . 32

5 Uncertainty Quantification 35
- 5.1 Computational Cost Reduction . . . 35
- 5.2 uncertainty parameters . . . 36
- 5.3 LHS results . . . 38
- 5.4 PCE Results . . . 40

6 Conclusions 45

7 Recommendations 48

References 49

A Model Flowcharts 54

B Chinook Model Inputs 55

C Plots with seperate experimental data 56

D Causes of PCE's limited accuracy 58

E Vortex-Ring Induced Velocity Formulation 60

List of Figures

1.1 A RNLASF CH-47F MYII CAAS Chinook helicopter. Image used with photographer permission © Ludo Mennes, Northern Skies Aviation . . . 1

2.1 Momentum theory inflow . . . 5
2.2 Momentum theory inflow in descent along with experimental measurements . . . 6
2.3 Helical vortex structure from a helicopter-rotor near hover (AeroDynamix 2012) . . . 7
2.4 Vortex wake structure in descent (Leishman et al. 2004) . . . 8
2.5 Example typical VRS boundary (Binet and Basset 2022) . . . 9
2.6 Fully developed VRS (Drees 1949) . . . 10
2.7 Schematic of the free wake model (Bagai and Leishman 1996) . . . 12
2.8 Inflow over two overlapping rotors (Chen et al. 2019) . . . 15
2.9 VRS boundaries determined with various criteria (Johnson 2005) . . . 17

3.1 Cross-sectional view: Position of vortex rings for different rates of descent . . . 19
3.2 Skewed wake of a helicopter in forward flight © Anton Filipenko via Vecteezy . . . 20
3.3 Thrust coefficient versus residual for different collective settings, using momentum theory 22
3.4 Augmented inflow model as proposed by Chen . . . 22
3.5 Chosen inflow model compared to experimental data . . . 23
3.6 Error due to blade element discretization . . . 24
3.7 Heave instability with RVM . . . 24
3.8 Erosion on a RNLASF CH-47F Chinook aft rotor blade (author's photograph) . . . 25
3.9 Flight dynamics based model of a rotor in descent . . . 26
3.10 Collective profile for a trimmed rotor in axial descent . . . 27
3.11 RNLASF CH-47F Chinook in hover or slow forward flight. Image used with photographer permission © Ludo Mennes, Northern Skies Aviation . . . 28
3.12 Overview of RVM components for the Chinook in hover . . . 29
3.13 Bifurcation applied to aft rotor ($\bar{V}_x = 0.5$) . . . 30

4.1 Predicted VRS entry and exit boundaries compared with ONERA and EASA experimental data (Taghizad et al. 2002; Binet and Basset 2025) . . . 31
4.2 Tandem and single rotor VRS bounds . . . 33

5.1 Error introduced by neglecting moments . . . 36
5.2 Error due to ignorance of trim in tandem configuration . . . 36
5.3 Vortex structure of a rotor deep in VRS (QinetiQ 2024) . . . 37
5.4 Convergence behavior of LHS sampling . . . 38
5.5 VRS bound samples with LHS . . . 39
5.6 95% certainty band of the VRS bound for a single rotor . . . 40
5.7 95% certainty band of the tandem-rotor VRS bounds . . . 40
5.8 Sample scatter ($\bar{V}_x = 0$) with first order polynomial fit . . . 41
5.9 Number of valid samples per bin . . . 42
5.10 Sample scatter with first order polynomial fit . . . 42
5.11 Cumulative Sobol indices . . . 43
5.12 Sobol indices per uncertainty parameter . . . 43
5.13 Comparison of LHS and PCE 95% certainty band . . . 44

A.1 Flowchart of the single-rotor model . . . 54
A.2 Flowchart of the multi-rotor model . . . 54

C.1 Predicted VRS entry and exit boundaries compared with ONERA experimental data (Taghizad et al. 2002) 56
C.2 Predicted VRS entry and exit boundaries compared with EASA experimental data (Binet and Basset 2025) 56
C.3 95% certainty band of the VRS bound for a single rotor (Taghizad et al. 2002) 57
C.4 95% certainty band of the VRS bound for a single rotor (Binet and Basset 2025) 57

D.1 Relation between VRS bounds and $\bar{V}_{peak}$ 59

List of Tables

5.1 Variances of uncertainty parameters 37

B.1 Rotor input parameters for the single- and tandem-rotor 55

Nomenclature

Abbreviations

Abbreviation	Definition
(e)VTOL	Electric vertical take-off and landing
BEM	Blade element momentum
BET	Blade element theory
CFD	Computational fluid dynamics
DHC	Defensie Helikopter Commando
DVTM	Dynamic vortex tube method
EASA	European Union Aviation Safety Agency
FMM	Fast multipole method
FWM	Free wake model
HOST	Helicopter overall simulation tool
KTV	Kantoor Testvliegen
LCT	Longitudinal cyclic trim
LES	Large eddy simulation
LHS	Latin hypercube sampling
MCS	Monte Carlo sampling
ONERA	Office National d'Études et de Recherches Aérospatiales
PCE	Polynomial chaos expansion
PDE	Partial differential equation
PIPC	Pseudo-implicit predictor-corrector
RNLASF	Royal Netherlands Air and Space Force
RVM	Ring vortex model
RVPM	Reformulated vortex particle method
TPP	Tip path plane
UQ	Uncertainty quantification
VPM	Vortex particle method
VRS	Vortex ring state
VTM	Vorticity transport method
VVPM	Viscous vortex particle method

Symbols

Symbol	Definition	Unit
A	Rotor disk area	[m^2]
B	Number of blades on a rotor	[-]
C_D	Drag coefficient	[-]
C_L	Lift coefficient	[-]
CT	Thrust coefficient	[-]
d	Number of uncertain parameters	[-]
E	Energy	[J]
k_Γ	Vortex-ring strength factor	[-]
k_{mi}	Mutual inflow factor	[-]
k_{ring}	Geometric vortex-ring inflow factor	[-]
m	Mass	[kg]

Symbol	Definition	Unit
$\dot{m}$	Mass flow rate	[kg/s]
N_{PCE}	Number of required samples for PCE	[-]
N_R	Number of radial blade elements	[-]
N_ψ	Number of azimuthal blade elements	[-]
N_{ring}	Number of vortex rings	[-]
P	Power	[W]
p	pressure or polynomial order of the PCE basis	[Pa] or [-]
R	Rotor radius	[m]
$\mathbf{r}$	Position vector	[m]
T	Rotor thrust	[N]
T_{shed}	Vortex-ring shedding interval	[s]
t	Time	[s]
$\mathbf{u}$	Velocity vector	[m/s]
V	Descent speed	[m/s]
V_{peak}	Descent speed with peak induced velocity	[m/s]
V_x	Forward velocity	[m/s]
v_i	Induced velocity	[m/s]
v_{i_0}	Induced velocity in hover	[m/s]
v_{con}	Convection velocity of the vortex rings	[m/s]
$v_{i_{mom}}$	Induced velocity from momentum theory	[m/s]
$v_{i_{peak}}$	Induced velocity at $\bar{V}_{peak}$	[m/s]
w_i	Induced velocity far downstream	[m/s]
x	Nondimensional radial distince from rotor centre	[-]
z	Nondimensional axial distance from rotor plane	[-]
Γ	Vortex-ring circulation	[m^2/s]
Δ_{ring}	Vortex-ring position offset	[m]
ζ	Coordinate along the vortex filament	[m]
ν	Kinematic viscosity	[m^2/s]
ρ	Air density	[kg/m^3]
ψ	Blade azimuth angle	[rad]
Ω	Rotor rotational speed	[rad/s]
$\boldsymbol{\omega}$	Vorticity vector	[s^{-1}]
$\bar{}$	Normalized by v_0	[-]

1

Introduction

1.1. Background and research objective

At a moderate rate of descent, with power applied and low/no forward speed, a helicopter can enter vortex ring state (VRS). During VRS, a large ring of vortices forms around the edge of the rotor, resulting in significant added induced inflow and hence power requirements, leading to an increase in rate of descent. Without the correct action taken by the pilots, the helicopter will continue to descend at an increasing rate. However, a proper recovery requires sufficient altitude, making VRS a potentially dangerous phenomenon close to the ground. Preventing the helicopter from entering VRS is therefore prefered. Hence, it is valuable to identify the flight conditions in which VRS occurs.

Historically, many helicopter accidents have been directly or indirectly attributed to VRS. Between 2008 and 2021, 48 accidents have been related to VRS, resulting in losses of airframes, bodily harm and even fatalities (Sotiropoulos-Georgiopoulos et al. 2023). Notably, the V-22 "Osprey" multi- and tilt-rotor platform encountered VRS in a descent deemed too steep. 19 lives were lost in the crash (Bolkcom 2005).

The Royal Netherlands Air and Space Force (RNLASF) is part of the Dutch armed forces and provides airpower both domestically and abroad. The Air Force's helicopters are assigned to the *Defensie Helikopter Commando* (DHC). The DHC operates, among others, the CH-47F MYII CAAS "Chinook" (Figure 1.1) and NH-90 NFH. The latter platform was unfortunately involved in a fatal accident near Aruba (Dutch Safety Board 2021). VRS was one of the hypothesized causes of the incident and since then, VRS has received increased attention within the DHC.



Figure 1.1: A RNLASF CH-47F MYII CAAS Chinook helicopter. Image used with photographer permission © Ludo Mennes, Northern Skies Aviation

The Chinook is a tandem-rotor platform; the helicopter has two counter-rotating rotors positioned one behind the other and therefore has no tail rotor. The aft rotor sits slightly higher than the front rotor, and the rotors tilt forwards, with the front rotor having a larger tilt. As a result, the two rotors partially overlap or even intersect. However, the two rotors are physically connected such that this intersection of the rotors does not cause a collision between the blades. It is unclear what effect this interference has on the onset of VRS. The model should thus incorporate interference in some way.

Within the Chinook Squadron, there is also more focus on VRS, although there is still no clear picture of the exact conditions in which the Chinook can enter VRS. The operator, 298 Squadron, is especially interested in the flight conditions causing VRS, as potential changes in flight training can then be implemented to improve safety. The manual of the Chinook currently does not mention VRS. The Flight Test Office or *Kantoor Testvliegen* (KTV) is tasked to determine the conditions in which VRS could be encountered. Specifically, the bounds of VRS are to be determined, which are the extreme combinations of forward speed and rate of descent where VRS is experienced.

Therefor, a model that determines in which conditions VRS can occur is desired, before actual flight testing commences. High fidelity models, rooted in computational fluid dynamics (CFD), are often computationally expensive. A simpler model that is able to determine the bounds of VRS with lower computational cost is preferable as the model is to be run many times for uncertainty quantification (UQ). A more complex model would rapidly become infeasible.

VRS is difficult to model as it is hard to simulate the structure of the vortices around the rotor. It is especially challenging to capture the randomness of the vortex structure, without adding so much fidelity that the model becomes too computationally expensive. The model used to describe VRS will hence carry some uncertainty, which may be quantified, for example by means of Monte Carlo sampling (MCS) or Latin Hypercube Sampling (LHS). However, for a relatively expensive model, a more efficient simulation like polynomial chaos expansion (PCE) could provide a sufficiently accurate result in less time. It is to be determined if PCE is appropriate for this application.

1.2. Research Question

The bounds of the VRS region for the Chinook are not known from literature. As discussed in section 1.1, the uncertainty is also an area of interest. Based on the identified research gap, the following main- and sub- research questions are formulated:

Main research question

Can VRS boundaries for single and tandem-rotor configurations be accurately predicted using the ring vortex model (RVM), and how do model uncertainties affect these predicted boundaries?

Sub-questions

1. How can a low fidelity rotor wake model, specifically RVM, be used to predict VRS boundaries for a single rotor?
2. How does rotor-rotor interference influence the predicted VRS boundary in a tandem-rotor configuration like the Chinook?
3. Which model parameters affect the uncertainty of the predicted VRS boundaries the most?
4. Is the uncertainty of the VRS boundary larger at specific (ranges of) forward speeds?
5. Can PCE, a potentially more computationally efficient method used for UQ, show adequate accuracy compared to LHS when applied to RVM?

Subquestion one aims to validate the use of a low fidelity method to investigate VRS in principle. Specifically for a single rotor, as test-data will be readily available. Subquestion two then aims to answer

if it is possible to expand the model to a multi-rotor platform, keeping the low fidelity model as a base. Typically, for multi-rotor platforms, higher fidelity models are used. With the answer to subquestion three, key model parameters are identified such that the UQ that will help to answer subquestion four, can be performed. To answer subquestion five, the simple sampling-based UQ is replaced by PCE, where fewer samples are fit to a polynomial. This fitting of a polynomial could cause a loss of accuracy in determining the uncertainty of the bound.

1.3. Scope

The VRS boundaries for the single and tandem-rotor are investigated through simulation. The simulation employs a low fidelity modeling approach. The rotor is modeled, but the wake is not a fully free wake. The wake is approximated by a prescribed vortex structure, with little 'freedom'. In the simulation, the helicopter is positioned upright, with its nose pointed in the direction of flight, such that sideslip is not specifically considered. Tilting of the helicopter around its pitch-axis is not explicitly considered either, albeit this is just a transformation of co-ordinates, i.e. the forward speed and rate of descent. Furthermore, the single- and tandem-rotors are analyzed at a singular weight, and design parameters are not altered. The tandem-rotor results are not validated due to a lack of validation data.

1.4. Outline

This thesis starts by giving an introduction and overview of the VRS phenomena including the historic and current research in chapter 2. Not all of this research is directly used later. The reader may decide to read only section 2.1 and section 2.8. The scientific background as described in chapter 2 is divided up into experimental observations (section 2.2), modeling approaches of VRS (section 2.3), additional models for inflow and rotor-rotor interference that supplement the VRS modeling (section 2.4 and background on UQ (section 2.7), before a knowledge gap is identified.

The methodology is described in chapter 3. The RVM is discussed in section 3.1, as well as its coupling to an inflow model, bound determination method and interference model in section 3.2, section 3.3 and section 3.4. Chapter 4 shows the results of the simulation and discusses initial conclusions. Most notably, the deterministic VRS bound is shown. The single rotor case is discussed first followed by the tandem-results, such that parallels and contrasts between both cases are more easily drawn. Finally, the UQ is shown in chapter 5, again starting with the single rotor cases. Concluding remarks and recommendations are given in chapter 6 and chapter 7.

2

Literature Review

VRS is an aerodynamic condition that any rotor [1] can encounter at moderate rates of descent, coupled with zero or a slow forward speed, and power applied. As the rotor blades create lift, they release a vortex at the blade root and tip. As the blades rotate around the rotor shaft, these vortices form a helical structure, contrary to a fixed-wing aircraft having the vortices trail straight back. At lower forward speeds, this vortical structure produced by the rotor blades remain around the rotor periphery. Combined with a moderate rate of descent, this helical structure starts to bundle and sit closer to the rotor, imposing significant downwash onto the rotor. This is analogous to induced drag on a fixed-wing aircraft and results in a significant increase in the induced power, which a typical helicopter cannot generate. Only the Sikorsky S-64 "Skycrane" is known to have enough power to simply pull out of VRS, when it carries no external load (Dziubinski and Stalewski 2007). In VRS, a helicopter experiences an uncommanded loss of altitude, and it does not necessarily automatically recover from VRS. The pilot experiences lower authority over the aircraft as well. This makes VRS a dangerous phenomenon.

VRS has been studied since the early days of the helicopter. In the earlier years, research was often experimental. In later years, modeling of helicopter rotors or even full helicopters has matured considerably, such that simulations are becoming the standard. Furthermore, especially multi-rotor research has become more relevant in recent years, with the rise of (electric) vertical take-off and landing ((e)VTOLs).

2.1. Vortex Ring State

To understand VRS, it is essential to understand the working principle of a helicopter rotor. In level and climbing flight, a helicopter stays aloft by sucking down air through its main rotor. This however changes in descending flight. With momentum theory, the operating states of a rotor, including VRS, are related in subsection 2.1.1.

2.1.1. Momentum Theory and Rotor Operating States in Vertical Descent

A rotor can be modeled by considering a stream of air passing through the rotor. Far above the rotor, this stream of air initially moves towards the rotor with a velocity equal to the rate of climb of the rotorcraft. The stream of air accelerates and passes through the rotor, where said rotor exerts a pressure jump on the stream. The stream of air then moves further down in axial direction. The rotor increases the momentum of the stream, hence the name momentum theory (Rankine 1865; Froude 1889).

Let V denote axial velocity of the air through the rotor (positive downward, so climbing flight) and $v_i > 0$ induced velocity at the disk (positive downward).

[1] When the word helicopter is used in this thesis, it can pertain a classic configuration helicopter, or any rotorcraft that utilizes one or multiple rotors for lift generation.

The normalized induced velocity $v_i/v_{i_0} = \bar{v}_i$ [2] is given by (Prouty 1995):

$$\boxed{\bar{v}_i = -\frac{1}{2}\bar{V} + \sqrt{\left(\frac{1}{2}\bar{V}\right)^2 + 1}} \tag{2.1}$$

At higher descent velocities, the rotor is driven by the flow instead of vice versa, such that momentum is transferred from the flow to the rotor, instead of vice-versa. This is called the windmill state, instead of the helicopter state as described before. Ultimately, this change results in the following (Prouty 1995):

$$\boxed{\bar{v}_i = -\frac{1}{2}\bar{V} \pm \sqrt{\left(\frac{1}{2}\bar{V}\right)^2 - 1}} \tag{2.2}$$

Note how for Equation 2.1 only one root is valid, as the inflow must be positive in hover and normal powered flight. Equation 2.2 has 2 solutions, but is actually only valid for rates of descent higher than 2 times the induced velocity in hover, or $\bar{V} \leq -2$.

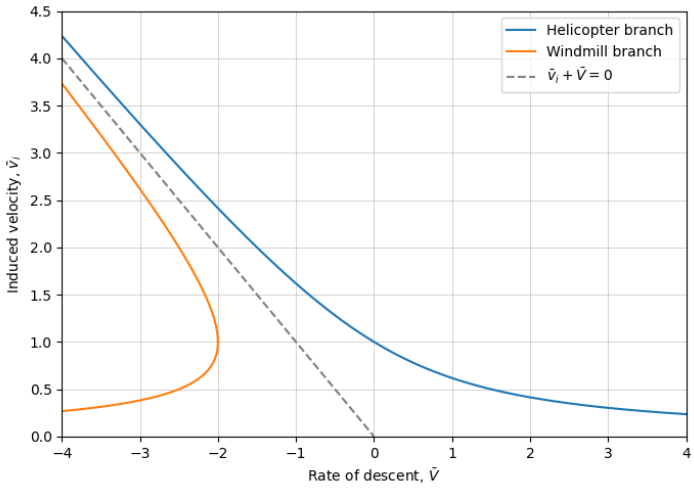


Figure 2.1: Momentum theory inflow

The plots indicating the induced velocity as per Equation 2.1 and Equation 2.2 are shown in Figure 2.1, along with a gray, dotted line indicating $\bar{v}_i + \bar{V} = 0$. This indicates zero net-flow through the rotor. The figure shows that there are 3 mathematically valid expressions for the induced velocity for $\bar{V} \leq -2$, while only one can physically occur under the assumptions of this derivation, as the stream of air has a single, uniform velocity at a given cross-section of said stream. Which of the three is correct, is to be determined using experimental data.

More interesting is however that there is a discontinuity between the branch corresponding to the normal working state and the windmill-state. Theoretically, the net flow through the rotor is close to zero here, as the gray dotted line shows. Indeed the rotor pushes air down, but the rate of descent is not high enough to actually result in a net-upwards flow through the rotor. The rotor encounters its own wake while descending and the wake curls up around the rotor, with the shed tip vortices bundling into a ring, forming a torus (commonly referred to as a 'donut-shape') of vortices around the rotor: VRS. This ring of vortices imposes a major downwash on the rotor, such that the net flow through the rotor is not zero as theoretically predicted. Instead, a rather large downwards flow onto the rotor

[2] The superscribt bar signifies that the velocity is normalized by the induced velocity in hover v_{i_0}. It is not exclusive to induced velocity but may also pertain to the velocity of a climb/descent or forward flight.

is present. This results in significant induced power, which full-size helicopters and similar do not posses as explained earlier in this chapter. Hence, VRS is also dubbed settling with power, though the more accurate term would be settling with insufficient power. Therefore, in this thesis the aerodynamic phenomenon will be referred to as VRS. VRS could result in a considerable uncommanded increase in rate of descent, a more 'sluggish' control, vibrations and thrust/torque oscillations (Prasad et al. 2004). Especially the undesired sudden increased rate of descent, the fact that the helicopter settles (i.e. does not automatically fall through the vortex ring to leave the state) and lesser pilot authority make it a dangerous phenomenon (Brand et al. 2007).

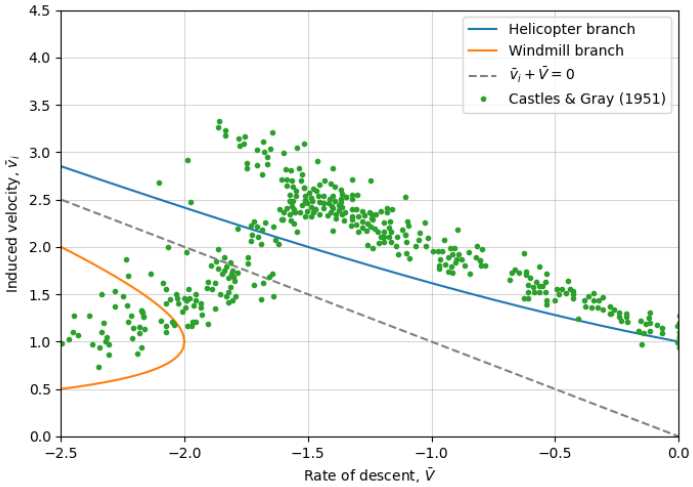


Figure 2.2: Momentum theory inflow in descent along with experimental measurements

Figure 2.2 shows the inflow according to momentum theory again, along with experimental measurements from Castles and Gray (1951) shown in green [3]. This experimental data is key to determine which of the three mathematical valid expressions is correct. The experimental data shows typically higher inflow than momentum theory predicts, at any descent speed. This can be explained by the tip vortices shed by the rotor blades imposing extra downwash, which are present even when not in VRS. At higher rates of descent, the experimental data indicates the lowest of the 3 solutions of the momentum theory is the most representative.

However, most important is the significantly higher induced flow in between the helicopter and windmill-state; indicative of the vortex ring state. From this data, it is unclear at what descent speed VRS starts exactly, but it is clear that it is most prominent around $\bar{V} = -1.5$. If momentum theory was to be used to model the inflow of a helicopter in descent, the helicopter branch is to be used up to approximately $\bar{V} = -1$, and the windmill branch is to be used starting at $\bar{V} = -2$. In between, around VRS, some transition and correction is required, as the prediction from momentum theory significantly diverges from the Castles and Gray data.

2.1.2. Qualitative Description of the VRS Phenomenon

With the concept of VRS introduced, the aerodynamic phenomenon is to be explored further. As a rotor in hover moves air to stay aloft, a vortex on the tip (and root, albeit less relevant) of the blade is shed and moved down with the wake. This vortex is shed as a high pressure zone is created under the blade, and a low pressure zone is created on top of the blade. At the tip, this causes a roll-up, i.e. a vortex, that is shed from the blade. A fixed-wing aircraft sheds tip vortices in a linear path behind it, but the rotating blades of a rotor form a helical structure of vortices (Figure 2.3).

[3] Data was extracted by digitizing a plot and can carry errors.

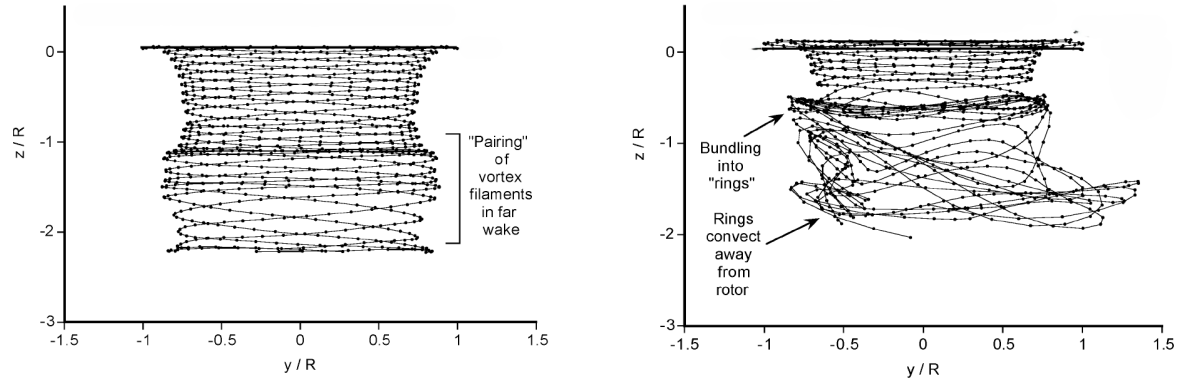


Figure 2.3: Helical vortex structure from a helicopter-rotor near hover (AeroDynamix 2012)

To show the significance of this vortical structure, the stream of air in hover can be interpreted as being a direct effect of solely the vortical structure. This vortical structure explains the increase in wake velocity as derived in subsection 2.1.1. The stream of air below the rotor is essentially surrounded by the vortical structure. The induction of these vortices is what accelerates the flow further downwards. The contraction of the wake that accompanies the acceleration is also explained, as the lower vortices induce an inward velocity on the upstream vortices. As these vortices move down, the upstream vortices counteract this effect, such that there is no indefinite contraction of the wake.

When comparing the rotor to a regular wing again, it is expected that the wake is so influential, albeit that it can be counterintuitive. For the trailing vortex that move in straight path behind a wing, the distance becomes ever larger, rather quickly. The influence of the vortices, that is the velocity they induce, reduces with distance. Only the closer, more newly shed vortices have a major influence. The bound vorticity on the wing itself is thus of larger importance than the wake. For a rotor blade however, that is essentially a rotating wing, the vortices stay closer to the rotor for longer, and this is clearly seen in Figure 2.3. The vorticity in the wake plays a relatively large role than the bound vorticity on the rotor blades, when compared to a wing of a fixed-wing aircraft.

Introducing a small rate of descent bundles the helical shape more tight, such that the vortices impose more inflow onto the rotor. However, the descent velocity of the helicopter, resulting in an apparent upward velocity of flow as seen from the rotor, more than compensates for this increased inflow. With a low rate of descent introduced, the lower vortices start to bundle up and somewhat expand, as shown in Figure 2.4a.



(a) Low rate of descent

(b) Increased rate of descent

Figure 2.4: Vortex wake structure in descent (Leishman et al. 2004)

A further increase in rate of descent causes the newly shed vortices to initially move upward before passing through the rotor and continuing downwards (Figure 2.4b. This introduces thrust fluctuations and vibrations, indicative of VRS developing. Furthermore, the increase in rate of descent compresses the helix even more, allowing for the pairing of vortices into a stronger ring below the rotor.

When the rate of descent is increased further, the ring may pass through the rotor as the rotor loses thrust. The rotor essentially falls through the bundled vortex ring. This event introduces large vibrations and fluctuations, as when passing through the ring, the rotor blades see fast fluctuations in local angles of attack. It is hence felt as the most significant, unsteady phase of VRS by the pilot. Nevertheless, this does not mean the rotor is rid of the vortex ring, as its position above the rotor does not necessarily mean it diverges from the rotor further.

Figure 2.2 shows a line with $v_i + V = 0$ and thus $\frac{\delta v_i}{\delta V} = -1$. On this gradient, there is no change in the sum of the freestream and induced velocity. This sum is the total inflow the rotor effectively 'sees'. For a more negative gradient, $\frac{\delta v_i}{\delta V} < -1$, an increase in descent velocity (having a positive effect on the rotor and its induced power), leads to a bigger increase in induced velocity. When connecting an increase of total 'seen' induced velocity ($v_i + V$) to a decrease in rotor thrust (which is true at a constant collective as the local angle of attack decreases), it is apparent how the region with $\frac{\delta v_i}{\delta V} < -1$, starting around $\bar{V} = -0.6$, is associated with the rotor falling through the vortices. One could argue that an increase in collective may counteract this and though in principal this is true, a rotor may not allow for excessive collective settings, let alone that the helicopter has the power to sustain this additional increase in induced power (Brand et al. 2007).

2.1.3. VRS in Forward Flight

In slow forward flight, VRS can still occur, although typically the range in terms of rate of descent at which VRS can occur, is somewhat smaller. The exact forward speed at which VRS ceases to occur is dependent on the helicopter and even its loading, but typically the forward speed V_x is less than the induced velocity in hover, or $\bar{V}_x < 1.0$ (Binet and Basset 2022). As the vortices move with the local flow, the introduction of a forward-speed component essentially blows the vortex ring structure back, away from the rotor.

An example of a VRS boundary is given in Figure 2.5. The boundary marks the extreme combinations of forward speed $\bar{V}_x$ and rate of descent $\bar{V}$ at which VRS is encountered. Within this boundary, marked in red, VRS is encountered as well.

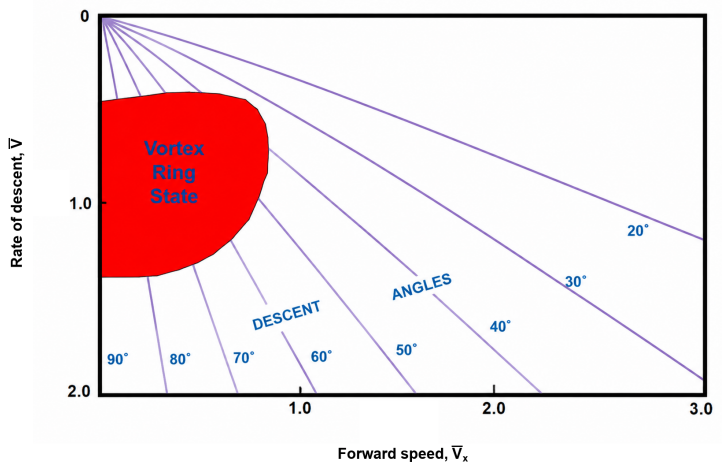


Figure 2.5: Example typical VRS boundary (Binet and Basset 2022)

The purple lines in Figure 2.5 showcase descent angles of the rotor and the figure shows how a more shallow descent angle would be needed to completely avoid VRS at any rate of descent. Important to mention is that the descent angle is relative to the rotor and not to a horizontal plane. A decelerating helicopter, tilting its rotor backwards to provide the 'braking' force, essentially experiences a large upward flow through the rotor and can thus encounter VRS conditions. This is true even for a shallow descent angle, or even without a descent.

2.1.4. VRS in Multi-Rotor Configurations

In a multi-rotor configuration, multiple rotors are positioned in the same/similar attitude, often negating the need for a tail-rotor as seen on conventional helicopters. Examples include tilt-rotors such as the Bell V-22 Osprey, tandem-rotors such as the Boeing CH-47 Chinook, co-axial helicopters such as the Sikorsky S-97 Raider or the relatively new eVTOL concepts, often having four or more propellers.

The V-22 Osprey has been extensively tested in VRS regimes after a deadly crash in 2000 (Bolkcom 2005). Not only the uncommanded increase in the rate of descent and fluctuating thrust was an important result of VRS, but the undesired 'roll-off' or asymmetric fluctuation of thrust causing a rolling motion of the aircraft, was especially dangerous (Mullen and Bernini 2016) For a co-axial helicopter this effect is not hypothesized to occur as the rotors are not horizontally offset, but for a tandem-rotor a sudden pitch, or for an eVTOL roll and/or pitch (depending on the placement of the propellers) can occur (Mori et al. 2025). In any case it is shown that rotor-rotor interaction has a significant effect on a rotor in descent, especially in VRS. Decreasing the lateral separation between rotors aggravates the interference (Chae et al. 2022). However, for co-axial systems it is suggested that VRS may be delayed to higher rates of descent with entry into VRS starting around $\bar{V} = -1.25$ instead of $\bar{V} = -0.5$, such that the interference between the rotors is advantageous in the context of VRS (Kinzel et al. 2019). For a tandem-helicopter such as the Chinook, the rotors partially overlap, such that either or a combination thereof could apply. Washizu et al. (1966) found little differences between their single rotor and tandem-rotors, although slightly higher thrust fluctuations were noted at a wider range of velocities. Brown (2024) noted that tandem-rotors show strong interference effects in VRS, even when the rotors are not overlapping. He found that VRS is envisioned to be encountered at lower rates of descent compared to a similar single rotor.

2.2. Experimental Observations

As any model will approximate reality and thus carry some error, experimental observations are essential to validate models. Furthermore, these observations can improve models with quantitative and qualitative information.

2.2.1. Single-Rotor Experimental Observations

Experimental data on the VRS phenomenon has been gathered since the early days of the helicopter. Johnson (2005) lists a wide variety of VRS data, starting at the work of Lock et al. (1926) (which Johnson deemed inaccurate) and Hafner (1948) (deemed guess-work). The first flight-test was done by Reeder and Gustafson (1949) on a Sikorsky R4, with Brotherhood (1949) later using the same type of helicopter to deduce the inflow on the rotor from various measurements, like (non exhaustive) weight, blade angle, and rotor speed. One limitation of Brotherhoods results was the lack of instability between inflow and rate of descent characteristic for VRS, as described in subsection 2.1.2. Drees (1949) visualized a rotor in various operating states including the VRS phenomenon, still often shown in reviews on VRS (Figure 2.6). Castles and Gray (1951) improved data from wind-tunnel testing with experience from Lock's work. Since then, many experimental investigations, both in windtunnels and flight-tests have been performed. However, windtunnels do not capture the 'drop' experienced in VRS like flight-tests do (Brand et al. 2007). Taghizad et al. (2002) present flight-test data from a Dauphin helicopter. More recently, research led by EASA in collaboration with *Office National d'Études et de Recherches Aérospatiales* (ONERA), the French national aerospace research institution, presented flight-test data on both a Dauphin and Fennec helicopter (Binet and Basset 2025).

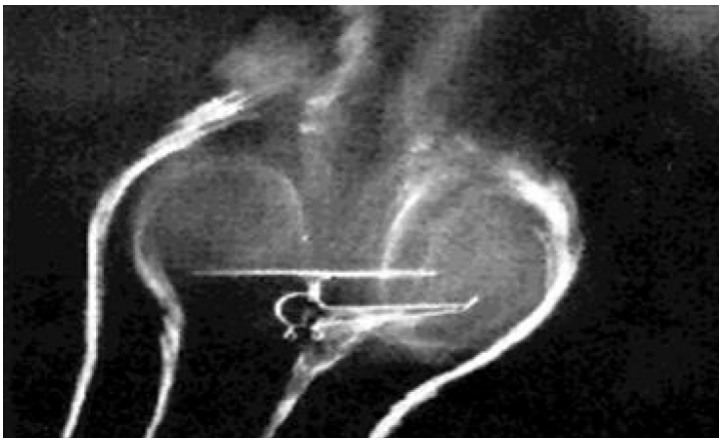


Figure 2.6: Fully developed VRS (Drees 1949)

2.2.2. Tandem, Coaxial, Tiltrotor, and eVTOL VRS Observations

Experimental investigations on multi-rotor platforms have also been performed. Yeates (1958) investigated a Piasecki HUP Retriever tandem-rotor helicopter, not unlike the Chinook. The research was mainly focused on vibration-levels, with the rotor-rotor interference causing significant vibrations in multiple flight-regimes. Vibrations in VRS are characterized as aperiodic. An investigation relevant to the Chinook is the work of Washizu et al. (1966), where a tandem-rotor was analyzed and compared to the same isolated rotor. Mainly, the tandem-rotors showed similar behavior, although thrust fluctuations were slightly larger and present in a larger part of the flight-envelope. More recently, an experimental study on eVTOL-like configurations has been performed (Veismann et al. 2021). However, it lacks specific comparisons between cases with and without interference, and results are often specific to a certain model, and not generalized. An investigation on a co-axial propeller did however compare to single rotors, and indeed results were similar as described in subsection 2.1.4, with the onset of VRS delayed to higher rates of descent (Marshall et al. 2024).

2.3. Modeling Approaches for VRS

With VRS qualitatively discussed and the importance of the shed vortices explained in subsection 2.1.2, various models developed to model VRS are to be discussed. General bounds for single rotors do not necessarily translate to multi-rotor platforms. These general bounds are not found in literature for these specific platforms. Hence, simulation is the more appropriate tool to find the bounds of VRS, i.e. the rates of descent and forward speeds at which VRS is expected to be encountered.

A distinction is made between high fidelity, mid fidelity and low fidelity models, with the latter sometimes referred to as fast models as they are not necessarily inaccurate. However, these fast models typically rely on relatively simple analytical expressions tuned for specific helicopters or holding empirical data in another way. They could thus not necessarily be suitable to predict VRS for multi-rotor platforms, but this is to be determined. Furthermore, they can be augmented to be an appropriate model for these multi-rotors and should thus not be excluded a priori. High fidelity models are typically CFD models and show good performance (i.e. the results generally align with experimental observations), but they do carry high computational cost. The mid fidelity models stand in between, trading off between accuracy and computational cost (Binet and Basset 2022).

2.3.1. Fast or Low Fidelity Models

Fast models are used to model the main effects of VRS, like the reduction in thrust, for example for the use in flight simulators. The wake is not explicitly modeled in detail. One of the most elementary methods is to simply match part of the inflow conditions (or speed and attitude) of the rotor to VRS, accompanied with a loss of thrust. However, this requires specific knowledge of when a platform will enter VRS, such that the bounds of VRS cannot actually be predicted. Simple momentum theory can be corrected for use in VRS by altering the mean inflow through the rotor in the VRS-region, which can then be coupled with blade element theory (BET). Studies show that simulated results match experimental flight data rather well (Binet and Basset 2022). However, inflow could also be modeled to vary locally, and various inflow models exist that can be applied to VRS conditions.

Empirical add-on to Momentum Theory

An inflow model developed at ONERA empirically adjusts momentum theory to give the mean inflow through the rotor (Jimenez et al. 2001). This method is in good agreement with the higher fidelity models from "helicopter overall simulation tool" (HOST) (Benoit et al. 2000), a multi-national effort to 'group' various rotor-analysis tools. Similarly, Johnson (2005) developed an empirical add-on to simple momentum theory to model the average flow through the rotor in VRS conditions, applying it to multi-rotor configurations as well. Though these models can provide sufficiently accurate results for applications like flight-simulation, they miss several characteristics of the phenomenon, most notably the lack of local variation in the inflow, such that for example aero-elastic effects cannot be accurately analyzed.

Ring Vortex Model

In the ring vortex model (RVM), the wake is not free, as opposed to many mid fidelity models. The wake is prescribed to consist of vortex rings with their radius equal to that of the rotor. They can move with the local flow, but do not break or deform into a non-circular ring, nor contract, expand or be situated in a plane that is non-parallel to the tip path plane (TPP). The helical wake being represented by vortex rings is particularly suitable in descent conditions. As the helical shape of the wake compresses, the error due to approximating a helical shape by a series of rings, diminishes. The model, developed by Chen (2006), supplements momentum theory. The rings superimposing inflow onto the inflow computed by momentum theory, is consistent with the observation that the inflow predicted by simple momentum theory is an underestimation, especially under VRS conditions (subsection 2.1.2). This model is one of the relatively higher fidelity models implemented into HOST. The model has been successfully applied to investigate VRS in a multi-rotor configuration, though only for axial descending flight and no oblique descent (Prasad and Chen 2006). In forward descending flight, the model has also been implemented for VRS analysis, although not for multi-rotor applications (Chen and Prasad 2005). Neither has been implemented for a set of overlapping rotors.

The simplification of the wake in VRS to a series of organized rings is not consistent with the wake of a tandem-rotor or even single rotor in developed VRS as shown by Brown (2024). However, this does not necessarily invalidate the model as a whole. Depending on the application, a simplified wake can accurately model VRS. As an example, for models rooted in flight-dynamics, the main effect to model is the increased inflow, which RVM does.

2.3.2. Mid Fidelity Model

The European Union Aviation Safety Agency (EASA) in their research on VRS (Binet and Basset 2022) speaks of the following mid fidelity models: free wake models (FWM), vortex particle methods (VPM) and vorticity transport methods (VTM), with the first two being examples of Lagrangian models and the latter Eulerian. Van Hoydonck et al. (2009) also differentiate between models with a free and prescribed wake, with the latter having its limitations. With a free wake, the wake does not conform to a prescribed topology. As the wake in a developed VRS is often of turbulent nature, a free wake aligns more with the wake in VRS. Here, there is another distinction between 'relaxation based' (periodic) and 'time-marching' (aperiodic) solution strategies. Enforcing periodicity of the wake can have a positive effect on the numerical stability of the simulation as the solution could otherwise not converge (Miller and Bliss 1993). However, Leishman et al. (2004) indicate that the wake in VRS is not stable and thus both spatially and temporally varying.

Free Wake Model

In a free wake model (FWM), vortices shed by the rotor are represented as lines or sheets. The tip-vortices are the most dominant aspect of the wake, especially in VRS conditions. As a result, the wake is now approximated by a series of lines, which have a distributed vorticity along them and stem from the tips of the blades as seen in the work of Bagai and Leishman (1996). The lines span between Lagrangian markers that move with the local flow. Figure 2.7 shows a singular blade releasing a vortex filament with some Lagrangian markers, referred to as 'collocation points'. The vortex filaments carrying the vorticity are named tip vortex filaments. Here, ψ is the blade azimuthal position and ζ the length across the filament.

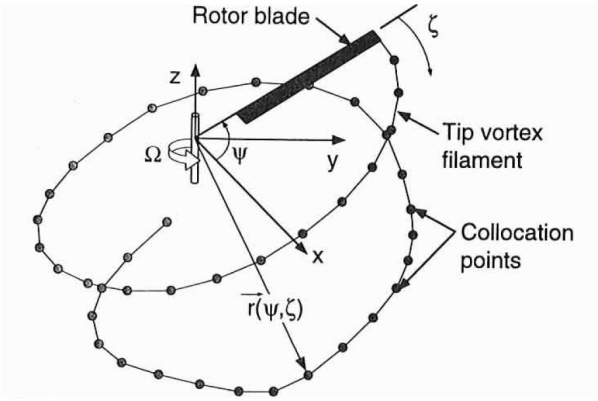


Figure 2.7: Schematic of the free wake model (Bagai and Leishman 1996)

As the markers move with the local flow, their velocity can be described as (Bagai and Leishman 1996):

$$\frac{d\mathbf{r}(\psi,\zeta)}{dt} = \mathbf{u}\big(\mathbf{r}(\psi,\zeta)\big) \tag{2.3}$$

or

$$\frac{\partial\mathbf{r}(\psi,\zeta)}{\partial\psi} + \frac{\partial\mathbf{r}(\psi,\zeta)}{\partial\zeta} = \frac{1}{\Omega}\,\mathbf{u}\big(\mathbf{r}(\psi,\zeta)\big) \tag{2.4}$$

Here, $\mathbf{r}(\psi,\zeta)$ is the position vector of a collocation point on the filament, t denotes time, and $\mathbf{u}$ is the local flow velocity inducing the motion of that point. This equation is a partial differential equation (PDE) with no simple analytical solution due to the nature of the right-hand side of the equation, such that it is to be solved numerically. Therefore, a discretization of the PDE is required such that the field can be solved for. Various approaches are taken, such as a pseudo-implicit predictor-corrector (PIPC) scheme commonly used by Bagai and Leishman (1996), while others use similar methods (Makeev et al. 2022). Furthermore, an inviscid vortex' velocity goes to infinite at the core, which is non-physical and should hence be avoided (Van Hoydonck et al. 2009). Various viscous vortex-core models exist

like the Rankine or Lamb-Oseen model that augment the induced velocity in the vortex core using empirical data (Van Hoydonck et al. 2009). As a result, even this mid fidelity model has some empirical parts.

Results from analyses with the use of FWM, specifically for multi-rotor applications, show good numerical stability and convergence characteristics. Although test data is not available for every configuration, some available data for a co-axial system shows the ability of the FWM combined with the PIPC scheme to capture the essential physical mechanisms of the twin-rotor model (Bagai and Leishman 1996) (Leishman and Bagai 1994). However, this is not focused on VRS. In FWM vortex filaments are truncated after some rotor rotations to limit the amount of collocation points, while in VRS vortex structures assemble around the rotor for longer times. The enforced periodicity of the wake is also not necessarily in alignment with a wake in VRS as Leishman et al. (2004) indicate. It is shown that the wake indeed shows some aperiodic behavior further downstream in hover, and the helical structure starts to bundle somewhat. However, this is consistent with experimental observations. The wake closer to the rotor seems stable, and the forced periodic and aperiodic methods show no significant differences. Increasing the rate of descent in the simulation shows further wake instabilities, and the vortex segments start to bundle into rings, indicative of VRS onset and again consistent with experimental observations.

Specific applications of this method are the MINT model developed at ONERA, or more recently the stand-alone PUMA [4] model (Binet and Basset 2022). The FWM has also been integrated into OpenFAST, a standard for wind-turbine analysis (Shaler et al. 2020). It has also been altered into a state-space model (Betoney et al. 2009), and though correlation with the earlier discussed finite difference FWM was generally acceptable, far-wake correlation was deemed unsatisfactory.

Vortex Particle Method

Vortex particle method (VPM), or sometimes dubbed viscous vortex particle method (VVPM), solves the vorticity-velocity forms of the Navier-Stokes equations. Starting from the incompressible Navier-Stokes, with pressure p, fluid density ρ and kinematic viscosity ν (Alvarez 2022):

$$\frac{\partial \mathbf{u}}{\partial t} + \mathbf{u} \cdot \nabla \mathbf{u} = -\frac{1}{\rho} \nabla p + \nu \nabla^2 \mathbf{u} \tag{2.5}$$

Taking the curl ω of velocity $\mathbf{u}$:

$$\frac{d\boldsymbol{\omega}}{dt} = (\boldsymbol{\omega} \cdot \nabla)\mathbf{u} + \nu \nabla^2 \boldsymbol{\omega}, \qquad \boldsymbol{\omega} = \nabla \times \mathbf{u} \tag{2.6}$$

Equation 2.6 states that the change of the vorticity in the field is the sum of the influence of the local flow-field on the vortices and its viscous diffusion. This way, artificial numerical dissipation as modeled by a vortex model is no longer required (Binet and Basset 2022). Another added advantage is that the wake is fully free compared to previously explained FWM, as the vorticity particles are not bounded by a linear segment. Furthermore, the Lagrangian nature of the method requires no grid as Eulerian methods do. A disadvantage is the rather large computational effort resulting from the large number of vortex particles needed (Van Hoydonck et al. 2009). It has been successfully used for multi-rotor applications (Zhao and He 2010; Singh and Friedmann 2021; Piccinini et al. 2021). VPM has also been used for simulations in VRS (Şenipek et al. 2023), showing good correlation with experimental results and general behavior of the simulated model is in agreement with typical observations during VRS. The non-prescribed form of the wake gives this method a relatively high fidelity, and the fact that it has been applied to VRS in a single-rotor application and multi-rotor application in the helicopter-regime, indicates that usage of the method on a multi-rotor application while operation in the VRS region is possible.

VPM can have some stability issues, especially when applied to unstable regimes like VRS. Therefore, a reformulated VPM (RVPM) was developed, in which vortex stretching is treated by allowing the

[4] The full meanings of the acronyms MINT and PUMA were not found by the author in the consulted literature.

vortex particles to change both strength and size, rather than only strength (Alvarez 2022). The new formulation acts as a meshless large eddy simulation (LES), while maintaining a computational cost similar to that of regular VPM. The formulation was extensively validated, and a multi-rotor test case showed "satisfactory agreement" with experimental data.

Vorticity Transport Method
With Vorticity Transport Method (VTM) the same vorticity-velocity form of the Navier-Stokes equations is solved, rather in a Eulerian frame of reference (Brown 2000).

$$\frac{\partial \boldsymbol{\omega}}{\partial t} + \mathbf{u} \cdot \nabla \boldsymbol{\omega} - \boldsymbol{\omega} \cdot \nabla \mathbf{u} = \nu \nabla^2 \boldsymbol{\omega} \tag{2.7}$$

Developments of this method have made the Eulerian grid to evolve with the vorticity and is thus Lagrangian-adjacent. The individual cells of this evolving grid are created and destroyed based on vorticity location, mitigating futile computations in a larger domain (Brown and Line 2005). A fast multipole method (FMM) reduced the computational cost from $O(N^2)$ to $O(N)$, substantially reducing computational effort with the large number of required vortices to model the wake.

The method is successfully applied to investigate VRS for single rotors, showing correlation to experimental data. VTM is especially suitable for VRS analysis as the Eulerian nature allows for vortices to stay around the rotor for many rotations, which aligns with experimental observations (Ahlin and Brown 2009; Ahlin and Brown 2005). Analysis on rotor-rotor interactions is also conducted, albeit a main-tail rotor interaction (Fletcher and Brown 2006) or co-axial rotors (Kim et al. 2009). However, no tandem or otherwise multi-rotor configuration with rotors laterally spaced, are analyzed. Nevertheless, the fidelity of these methods without prescribed wake, allows for freedom in the chosen configuration and the positive results from this method should carry over to other configurations.

2.3.3. High Fidelity Models

High fidelity methods pertain computational fluid dynamics (CFD) methods, where often accurate results come with the burden of high computational cost. Hoinville and Renaud (2007) analyzed a single rotor in VRS using CFD, while Castellin (2005) used CFD to investigate the applicability of wind-tunnel testing to VRS. An example of CFD used in multi-rotor analysis is the work on a multi-rotor UAV operating in VRS near a ground vehicle (Hahn et al. 2025), or NASA's DragonFly (Marshall et al. 2024). The versatility of CFD methods is shown by the various cases that are analyzed (hover, near-ground, VRS) with the same model (Lewis et al. 2023). CFD represents the most physically accurate approach, albeit at computational costs that prohibit its use within an uncertainty quantification framework.

2.4. Inflow Modeling

In section 2.3, various models are discussed to model the VRS phenomena. In some cases, these models are to be supplemented by other models. As an example, RVM improves simple momentum theory. However, it can also be coupled with BET. A radially and/or azimuthally varying inflow model can then be used, which more accurately models the inflow through a real rotor. This would allow to include more local effects of rotor-rotor interference.

Momentum theory as derived in subsection 2.1.1 is the most elementary inflow model used in helicopter performance analysis. Its power lies in its simplicity and that it is purely analytically derived. However, it only describes the average inflow over the disc, while in maneuvering or forward flight, the inflow is no longer uniform.

Pitt-Peters
The Pitt-Peters inflow model (Pitt and Peters 1981) is a 3-state inflow model, dependent on the loading of the rotor. The average inflow through the rotor, corresponding to the first state of the 3-state model, is equal to momentum theory. The second and third state correspond to the lateral and longitudinal tilt of the magnitude of the inflow over the rotor. Like the average depends on the thrust produced by the

rotor, the tilt depends on the moments the rotor generates around the roll and pitch axis. Furthermore, the tilt around the lateral axis increases with forward speed.

Peters-He
The Peters-He model is a finite state induced flow model that has a varying inflow over both the radial and azimuthal direction. It offers flexibility to the user, as any number of blades, and any angle of attack of the rotor disc can be chosen. Furthermore, it allows for the user to choose the (for example) amount of radial shaping functions, such that the detail of the inflow variation can be altered as desired. As the original model implies a skewed wake and thus does not model wake roll-up, the model is not valid for the VRS region (Peters and He 1995). However, the model was improved to include the VRS region by He et al. (1999), later discarded for an easier and more flexible method by Peters and He (2006). This improved Peters-He inflow model has also been applied in a multi-rotor scenario, more specifically a co-axial rotor system (Prasad et al. 2012). Interference between the rotors is determined by integrating the derivative of the individual pressure potentials from infinity to the other rotor disk, along the stream-line. The streamline in VRS conditions however is not well defined, such that this method does not necessarily translate to VRS for multi-rotor cases. The Peters-He model has been further developed. The model has been expanded to describe a three-dimensional flow-field, and convergence behavior has been improved (Hsieh and Peters 2005).

2.5. Rotor-Rotor Interference

Some of the models discussed in section 2.3, like empirical add-ons to momentum theory, pertain only to single rotors. For models that model the wake in some detail, rotor-rotor interference is inherently included. The wake stemming from one rotor is simply imposed onto the other rotor. Some models however do not model the wake explicitly, or in smaller detail. Again taking RVM as an example, the rings are a crude simplification of the vortical structure of the wake. It can be required to model the rotor-rotor interference in more detail. Both inflow and interference models are to be discussed.

For multi-rotor applications, the inflow as prescribed by any of the models from section 2.4 is to be super-positioned not only by the effect of the vortex structure as is predominant in the VRS. It is also to be corrected to include rotor-rotor interference. Especially for overlapping rotors like a co-axial or tandem configuration (like the Chinook), this interference is significant (Figure 2.8, subsection 2.1.4).

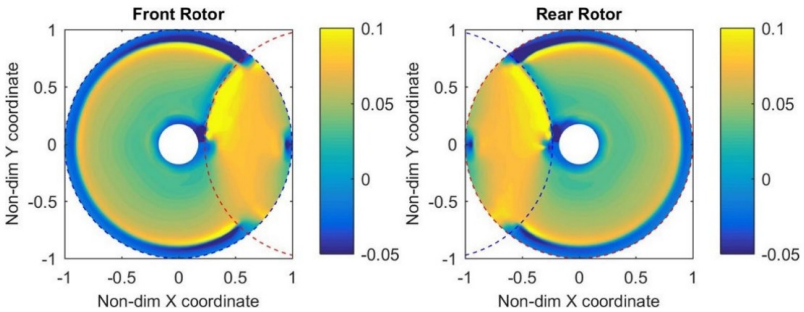


Figure 2.8: Inflow over two overlapping rotors (Chen et al. 2019)

In this century, research on rotor-rotor interference is often performed with the use of CFD based methods as their high fidelity provides flexibility to the configurations that can be analyzed. CFD based methods give results that are generally in agreement with validation data (Zhao et al. 2025; Hayami et al. 2020). Likewise, when a CFD-adjacent method like VPM is used to model a rotor in VRS, these interferences are inherently incorporated. However, as also described in section 2.3 in relation to VRS modeling, these models are computationally expensive. This is especially be problematic when the model is desired to be used in real-time for example, or is to be run frequently in relation to UQ. For lower fidelity methods that do not necessarily model the entire wake of the rotor, the interference will have to be explicitly incorporated some other way. Sheen et al. (2023) use blade element momentum theory to analyze the interference between two intermeshing rotors. The induced velocity of both rotors is computed separately. After, the induced velocity of rotor A is superimposed onto the part of rotor B

that sits under said rotor, and vice versa.

Alternatively, the dynamic vortex tube method (DVTM) has been used to model multi-rotor systems, both non-overlapping (Park et al. 2023) and overlapping (co-axial) (Choi et al. 2025). With DVTM, the wake is approximated as a continuous tubular sheet carrying vorticity, not unlike RVM (section 2.3). The model focuses on the shed tip vortices, with the results integrated to determine the coefficients of the state-space inflow model that represents said situation. Furthermore, more or less states, translating to more or less detail in the local inflow variation, can be taken based on the desired level of detail.

Nevertheless, DVTM is not a VRS model, even though the vorticity shed by the tip vortices is an essential part of the method. Its relevance lies in the more general concept. The wake is approximated, and the interference is modeled by computing the effect of the wake of one rotor onto the other. In this thesis, the idea of representing the wake in some simplified form like in the RVM, and superimposing the effects of this wake onto each rotor of the aircraft, can be widely applied.

2.6. VRS boundary determination

Not every rotor model is capable of simulating a rotor in VRS. For example, simple momentum theory coupled with BET is no longer valid in VRS, as the assumed continuous flow through the rotor disk breaks down. Models such as RVM and FWM allow a rotor to be analyzed both inside and outside VRS, but do not inherently indicate when the rotor enters the VRS regime. The boundary around the VRS region, expressed in terms of forward speed and rate of descent, is to be determined.

The heave instability as readily discussed in subsection 2.1.2 determines the bounds of VRS as an increase in average inflow through the rotor when the rate of descent is increased, as this would decrease the thrust produced by the rotor, increasing the rate of descent (Binet and Basset 2022). Similarly, the rate of descent itself or the thrust themselves can be analyzed, which are all closely related. In essence, this is the same criterion and some refer to each of these methods as heave instability (Basset et al. 2008). Criteria can also be based on unsteadiness of various parameters in the simulation (Johnson 2005). For example, Washizu et al. (1966) focused on thrust fluctuations, while Yeates (1958) looked at excessive general vibrations of the airframe.

Alternative to these criteria based on fluctuations, Newman et al. (2003) described the brake-down of the wake in VRS. Similarly, Basset et al. (2008) discussed a criterion based on zero transport velocity of rotor tip vortices, which marks the brake-down of the rotor-wake moving downwards as in the helicopter state. In the same paper, they describe the bifurcation criterion, introduced by Prasad et al. (2004). Here, VRS is marked as a reversal in the relation between the rate of descent and the collective. In the helicopter state, a decrease in the rate of descent would be paired with a decrease in the required collective to produce the same amount of thrust. In VRS, the increase in inflow that the rate of descent introduces causes the need for a higher set collective, such that this method is analogous to the heave instability.

Literature shows considerable variation in the predicted VRS boundaries when different criteria are applied (Figure 2.9). This does not necessarily indicate a deficiency in any of these criteria, as they may represent different physical phenomena associated with VRS. Consequently, as a helicopter approaches VRS, one VRS-related phenomenon may occur before another, resulting in different identified boundaries.

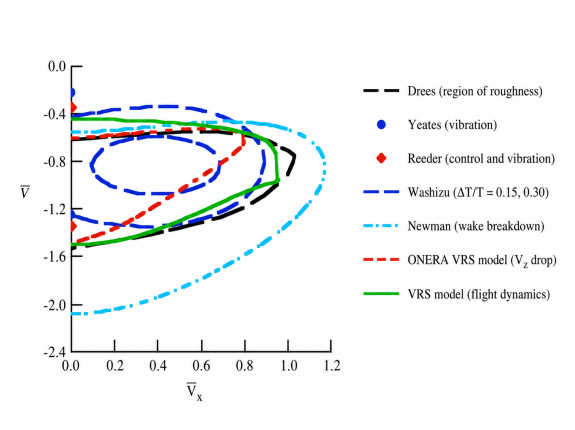


Figure 2.9: VRS boundaries determined with various criteria (Johnson 2005)

2.7. Uncertainty Quantification

Simulations are a powerful tool to analyze helicopter performance before requiring flight-testing. The value of such a simulation lies in its ability to accurately model a helicopter, which can be lower than desired due to uncertainties. Especially epistemic uncertainties stemming from insufficient knowledge of the system or model assumption to (for example) reduce computation effort, are important (Radcliff and Pavel 2025). Low fidelity models (section 2.3) hold epistemic uncertainties, almost by definition, as they can be considered to deliberately ignore knowledge on a rotor in VRS, to considerately simplify the model. In order to analyze the influence of uncertainties in the modeling of VRS on the predicted VRS bound, an uncertainty quantification (UQ) must be performed. Vouros et al. (2019), analyzing rotor aero-acoustics, show a 12% uncertainty when there is experimental data available to adjust their vortex core model. In absence of this data, a 25% uncertainty is found. Considering that low fidelity models for VRS often use experimental data, a UQ becomes especially relevant. Though it is clear that the exact bounds of VRS are uncertain and many studies predict different bounds (Binet and Basset 2022), an actual UQ on VRS is lacking.

Yuan et al. (2022) analyzed the uncertainty of a tilting multi-rotor. Instead of aerodynamic coefficients or geometry of the aircraft, the uncertainty of the aerodynamic model itself was analyzed. This is relevant for one of the lower fidelity models for VRS, as the experimental data in these models will carry uncertainty. Another example of UQ on multi-rotors is the research of Jayaraman et al. (2022), varying input conditions as freestream velocity and wind direction.

2.7.1. Sampling-based Uncertainty Quantification

A simple sampling-based uncertainty propagation is the most elementary approach to quantify the uncertainty of a system, or in this case model. Parameters that carry uncertainty are assigned a probability distribution. The model is then applied repeatedly with these parameters varied. If the model indeed carries uncertainty, the output will show a distribution as well. This distribution can then be analyzed and summarized, by showing the mean, median, confidence bounds, etc.. In the context of VRS, the output of the model is the predicted VRS bound.

The most simple sampling approach is Monte Carlo sampling (MCS). In MCS, samples are drawn randomly from the prescribed input distributions. This makes the method general, and it can be applied to any model, even if non-linear or non-smooth. However, MCS is inefficient, as a large number of samples is often required to achieve a representative spread over the uncertainty parameters. This can become computationally expensive when each sample requires a full rotor simulation. Siva et al. (2011) apply MCS to quantify the uncertainty of helicopter performance based on uncertain aerodynamic (lift- and drag-profiles) and geometric characteristics of the blade. Power required is increased by about 5 to 10%, with a probability of 10 to 12%. 100.000 samples are used.

Latin hypercube sampling (LHS) can be an improvement compared to MCS, as the uncertainty parameters are divided into intervals, with a equal probability of a sample being attributed to a certain interval (McKay et al. 1979). This gives a more even spread of the uncertainty parameters. LHS is especially valuable at a low number of samples, such that it is preferred over MCS with expensive models, when computing more samples is not feasible. Khurana et al. (2023) used 500 samples to investigate trends between blade stiffness uncertainties and rotor responses. Though this number is not to be compared directly to the 100.000 samples used with MCS as they stem from different studies and, for example, the amount of uncertainty parameters differs.

2.7.2. Polynomial Chaos Expansion

Instead of evaluating the same model numerous times at only slightly different input parameters, it can be advantageous to synthesize a surrogate model that replaces the original model, if this surrogate is less computationally expensive. With polynomial chaos expansion (PCE), samples are gathered and orthogonal polynomial functions are fit to these samples. When the model consisting of said polynomials is synthesized, it can be evaluated many times at a fraction of the cost. PCE has shown to achieve a 98% reduction in computational time, compared to MCS (Radcliff and Pavel 2025).

Although PCE has not specifically been applied to VRS, there are examples for general rotor simulations, including multi-rotor systems. Anusonti-Inthra et al. (2019) applied LHS and PCE to a co-axial rotor, showing results that are generally in agreement with each other. Vouros et al. (2019) use PCE to perform UQ on noise levels generated by a helicopter, which is surprisingly relevant to VRS as he applied a FWM to model the rotor in flight.

2.8. Summary and Knowledge Gap

This chapter discusses background theory on, as well as developments in VRS research, for single- and multi-rotor configurations. Momentum theory is used to explain the working principle of a rotor and shows a discontinuity between the normal working state and the windmill brake state. Experimental observations show increased inflow through the rotor, indicative of VRS. The wake in VRS is characterized as well. In forward flight, the wake is convected away from the rotor, decreasing the range of rates of descent at which VRS occurs. In multi-rotor configurations, VRS becomes more complex because the wake of one rotor can influence the inflow of another rotor and vice versa. Depending on the rotor layout, this interference may accelerate or delay VRS onset, or introduce asymmetric thrust fluctuations introducing undesired pitch- and/or rolling moments.

Literature shows that VRS can be modeled with different levels of fidelity. High- and mid fidelity models are able to model the wake in more detail, but their computational cost makes them less suitable for repeated evaluations as required in UQ. Low fidelity models can be attractive due to their lower computational cost. However, these models often rely on experimental data. Furthermore, they often heavily simplify the wake, key in VRS, if it is even modeled at all. Nevertheless, it is important to remember that a model simplification does not necessarily result in less accurate outcomes (Binet and Basset 2022).

The main identified knowledge gap is the prediction of the VRS boundary for a tandem-rotor helicopter, specifically the Chinook, with a lower fidelity model. Open literature does not show that any of the described methods have been applied to the Chinook, but RVM has been applied to multi-rotor configurations, although those rotors did not overlap. However, this pertained to axial descent only and RVM is yet to be applied to a multi-rotor platform in forward flight. A second identified knowledge gap relates to UQ, which has also not been performed yet on VRS, neither for single-rotor nor multi-rotor platforms. This is especially relevant when a low fidelity method is used.

By combining a computationally efficient low-fidelity rotor model with UQ, this thesis aims to determine both the nominal VRS boundary and the uncertainty introduced by modeling assumptions, thereby addressing two clear research gaps.

3

Methodology

Lower fidelity models may not capture the key aerodynamic mechanisms governing VRS, because they do not accurately represent the rotor wake, one of the defining features of VRS. Higher fidelity models incur a high computational cost, which is especially problematic when the model is to be run frequently during UQ. The objective of the methodology is not to maximize physical fidelity, but to maximize predictive capability within a computational budget compatible with uncertainty quantification. As a compromise between computational cost and physical fidelity, the ring vortex model (RVM) as developed by Chen (2006) (briefly introduced in subsection 2.3.1) is chosen. The model is a low fidelity model, but sits closer to the mid fidelity models than other low fidelity models, like those that solely apply empirical relations to momentum theory. This lack of empirical relations that are specific to certain platforms or even specific types of helicopters, makes RVM better suited for new configurations. The wake is modeled by a series of vortex rings released by the rotor. These vortex rings are explicitly modeled, but are fairly 'rigid', meaning they can only move downwards and forwards, while they can not tilt, deform, break, expand, etc.. The assumptions of this methodology are listed in section 3.5. The structure of the computational workflow is presented in Appendix A. The single-rotor configuration analyzed in this chapter demonstrate the methodology represents one of the Chinook's two identical rotors. For the tandem-rotor cases, both Chinook rotors are modeled (Appendix B).

3.1. Ring Vortex Model

As discussed in subsection 2.3.1, the rings of RVM only move in two dimensions, namely forwards and downwards. In hover, the rings move downward with the induced velocity of the rotor. Figure 3.1a qualitatively shows the position of the vortex rings in hover, descent, and a faster descent. The figure is a cross-section as seen from the side. The red line represents the rotor, from which the rings are shed. The vortex rings are represented by two circles each with a rotational direction.



(a) $\bar{V} = 0$ (hover) **(b)** $\bar{V} > -1.5$ **(c)** $\bar{V} < -1.5$

Figure 3.1: Cross-sectional view: Position of vortex rings for different rates of descent

With an increasing rate of descent, the vortex rings are not only convected by the downwash of the rotor. The upflow as introduced by the descent adds to the downwash of the rotor, such that the velocity of the vortex rings relative to the rotor decreases. This causes the rings to be situated closer to the rotor disc (Figure 3.1b). The velocity of the rings is thus the result of two contributions; that of the induced flow and that of the upflow due to descent. At a certain rate of descent, the VRS phenomenon will be

the most prominent. The vortex rings introduce the most inflow at a certain point when this point is situated closer to the rings. Therefore, the rate of descent at which VRS is the most prominent, must coincide with the moment the vortex rings coincide with the disc circumference in this model. This point, determined from experimental data (Chen 2006), is $\bar{V}_{peak} = -1.5$. Between this point ($\bar{V} = -1.5$) and hover ($\bar{V} = 0$), this contribution to the rings' velocity, due to the introduced rate of descent, is linearly interpolated (and extrapolated outside of this interval, corresponding to Figure 3.1c). It is added to the other contribution; the induced velocity v, to find the convection velocity of the rings v_{con} (Chen 2006):

$$v_{con} = v_i - \frac{v_{i_{peak}}}{\bar{V}_{peak}} \bar{V} \tag{3.1}$$

$v_{i_{peak}}$ is the induced velocity at V_{peak} and would also have to be determined using experimental data.

If the helicopter were to have a forward velocity, the vortex rings are blown back relative to the rotor with the helicopters forward velocity. This results in a skewed wake. Figure 3.2 qualitatively shows the positions of the gray vortex rings in forward flight.

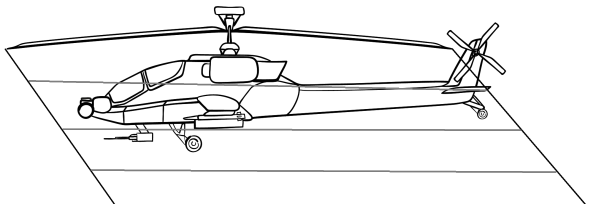


Figure 3.2: Skewed wake of a helicopter in forward flight © Anton Filipenko via Vecteezy

In a normal (non-VRS) flight-regime, the vortex rings are a simplification of a helical structure of tip vortices released from the blade tips. In the VRS-regime, they are a simplification of an often complex structure of interfering vortices, especially as VRS starts to develop (QinetiQ 2024). Modeling this more complicated structure requires a higher fidelity model, which has been avoided in this thesis to limit computational cost. However, the individual rings bundle into a single, more chaotic ring that carries more vorticity (subsection 2.1.2). Therefore, the wake in VRS can still be modeled by a series of these vortex rings, as they are situated closely to each other (Figure 3.1). Some aspects like the turbulence are ignored, but the main effect of increased inflow is modeled.

Every blade sheds vortices, such that they all have a single helical structure it deposes into the wake. Translating this to intermittent rings, a ring is shed per every full rotation of a blade. With B the number of blades on a rotor, the interval of a ring being shed (T_{shed}) by the rotor is given by (Chen 2006):

$$T_{shed} = \frac{2\pi}{\Omega B} \tag{3.2}$$

Here, $\Omega[rad/s]$ is the rotational speed of the rotor.

However, the position of the first vortex ring is not simply the product of its convection velocity and the shedding interval. The ring will also have moved from the rotor to this position and thus held every position in between at some point. As the proximity of a vortex ring to the rotor influences the effect (added inflow) said ring has, it is key that this effect is captured. An amount of samples can be taken with one ring per sample positioned anywhere in this interval, uniformly distributed. Afterwards, the value of the added inflow each ring position predicted, can be averaged. This still results in an inflow-correction that is constant over time, while being somewhat more accurate. The positions are

sampled sufficiently densely to achieve convergence within 0.02% as adding more samples is relatively computationally expensive. Five samples were found to be sufficient. With the position of the rings determined, their strength and resulting inflow field is to be known. the strength of the vortex ring Γ is given by (Chen 2006):

$$\Gamma = k_\Gamma R v_i \tag{3.3}$$

It is assumed that the inflow v is the uncorrected value from momentum theory and thus does not require an iteration after the vortex ring increased the inflow. k_Γ is a to be determined factor. R is the radius of the rotor. The increment of the induced flow is determined by (Chen 2006):

$$\Delta v_i = k_{ring} \frac{\Gamma}{R} \tag{3.4}$$

which is an average over the rotor disc. The geometric factor k_{ring} is determined from the work of Castles and De Leeuw (1953), in which the average and local flow-field around a vortex ring is described (Appendix E).

With the definition of the added induced flow being $v_{peak} - v_{mom}$ at $\bar{V} = -1.5$, this can be equated to Equation 3.4, with Equation 3.3:

$$v_{i_{peak}} - v_{i_{mom}} = k_{ring} \frac{k_\Gamma R v_{i_{peak}}}{R}$$

$$k_\Gamma = \frac{v_{i_{peak}} - v_{i_{mom}}}{k_{ring} v_{i_{peak}}} = \frac{\bar{v}_{i_{peak}} - \bar{v}_{i_{mom}}}{k_{ring} \bar{v}_{i_{peak}}} \tag{3.5}$$

with $\bar{v}_{i_{peak}} = 2.5$, $\bar{v}_{i_{mom}} = 2.0$ and $k_{ring} = 0.75$, $k_\Gamma = 0.2667/N_{ring}$ according to Chen (2006). $v_{i_{mom}}$ is the induced velocity through the rotor according to momentum theory, opposed to $v_{i_{peak}}$ which is experimentally determined. The amount of vortex rings is prescribed to be two as this aligned best with experimental data.

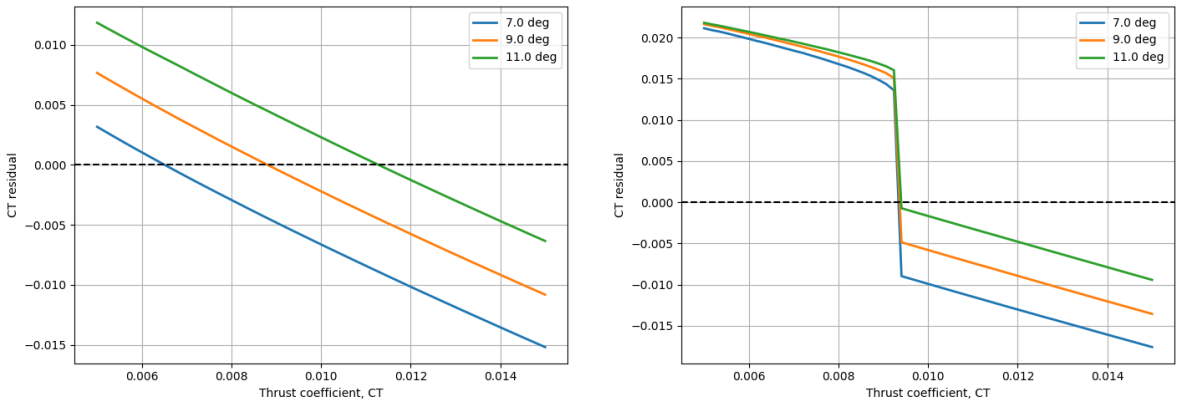
3.2. Inflow Model and Blade Element Theory

The original momentum theory (subsection 2.1.1) can be used as an inflow model in combination with a discretization of the rotor in radial and azimuthal direction, blade element theory (BET). With this discretization, every section can be analyzed with 2D airfoil data, after which results can be summarized over the entire rotor. Chen uses momentum theory as a baseline in his model. However, VRS occurs right around the most troubled part of momentum theory. The assumption of a continuous stream of air going through the rotor ceases to be valid, and VRS occurs between the helicopter- and windmill-branch of momentum theory (subsection 2.1.1). A smooth transition between both branches is needed. This need is apparent when blade element is used in conjunction with momentum theory without a smooth transition.

The helicopter branch is used for $V > -2$, for $V \leq -2$ the windmill branch is used. The rotor is to be trimmed, such that it produces 1G of thrust. This can be achieved by selecting the proper collective setting. The inflow depends on the thrust and as this inflow influences the local angle of attack on each blade section, it in turn influences the thrust. A certain desired CT [1] is thus to be selected, after which the resulting CT is to be computed. These CT values are however to be consistent with each other, i.e. the residual between them should be zero. With the proper collective, as a larger collective leads to a larger local angle of attack across the blades and thus larger thrust, this can be achieved.

[1] Nondimensional thrust coefficient, $CT = \frac{T}{\rho \pi R^2 (\Omega R)^2}$

Figure 3.3 shows the desired CT against its own residual (i.e. how much it diverges from the desired thrust to be consistent with itself) for a range of arbitrary collective settings. Figure 3.3a shows the relation in hover and Figure 3.3b for $\bar{V} = -2$, where the unnatural transition takes place:



(a) Hover

(b) $\bar{V} = -2$

Figure 3.3: Thrust coefficient versus residual for different collective settings, using momentum theory

Figure 3.3b shows each and every collective setting leads to the desired consistency, or in other words it is completely insensitive to the collective inputs. Figure 3.3a shows that each and any collective setting gives a single CT value, such that a singular collective setting causes trim of the helicopter. The shown insensitivity to the collective around $\bar{V} = -2$ shows a clear need for an augmentation.

An augmentation of the inflow model is postulated (Chen 2006), which connects the helicopter- and windmill-branches of momentum theory in a smooth manner for any forward speeds at which the jump in momentum theory occurs. However, with forward flight the magnitude of the inflow over the disc tilts in longitudinal direction, and when the rotor creates a moment, the inflow tilts in lateral and/or longitudinal direction. A state-space inflow model, with the states allowing for this local variation of inflow, could be a more accurate representation of the actual inflow. Chen proposes augmented state-space inflow models, giving one of three and seven states. However, these models seem flawed as they still show non-smooth behavior (Figure 3.4) and are not accompanied by further reasoning.

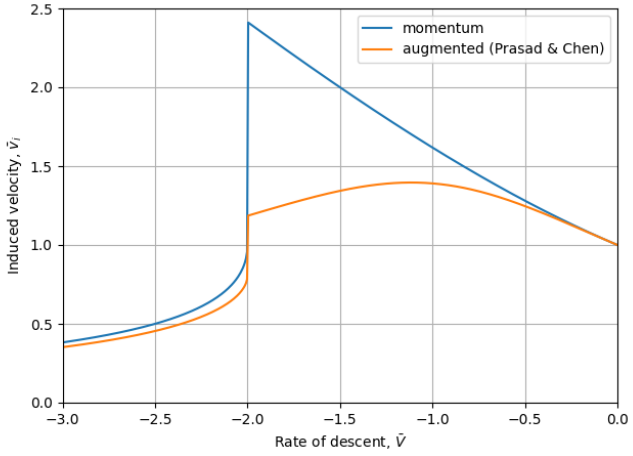
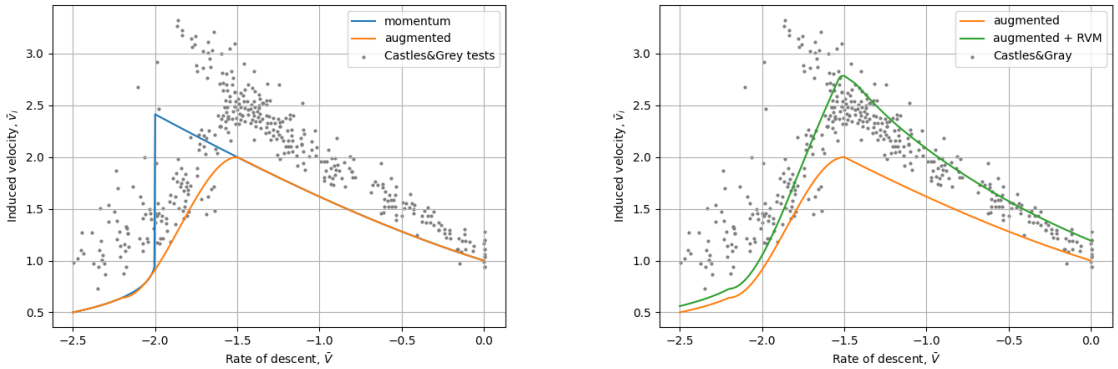


Figure 3.4: Augmented inflow model as proposed by Chen

Therefore, it is preferred to alter an existing inflow model. As the main phenomenon to capture is the tilt

of the inflow in forward flight, the 3-state Pitt-Peters inflow model (section 2.4) is an appropriate inflow model. The first state of Pitt-Peters, which is the average inflow over the disc, is equal to momentum theory. As such, the first state is to be altered, while the second and third state, corresponding to the disc tilt, are not changed. A simple but smooth interpolation is implemented between two certain points on the helicopter and windmill branch (Figure 3.5a). The bounds of the interpolation are determined by comparison to test-data from Castles and Gray (1951) [2], who derived the induced velocity in descent from wind-tunnel force tests on four model rotors. The bounds are taken as $[-2.2, -1.5]$.



(a) Augmented momentum theory

(b) RVM applied

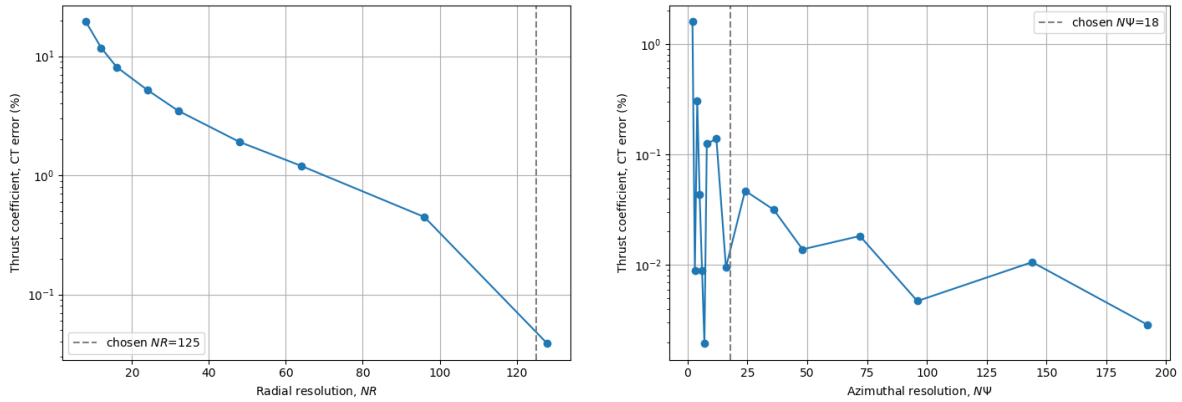
Figure 3.5: Chosen inflow model compared to experimental data

RVM can now be applied and compared to Castles and Gray data (Figure 3.5b). The figure shows how there is a peak of inflow around $\bar{V} = -1.5$, as expected. Furthermore, the inflow resulting from RVM generally shows the same trend as the experimental data. At lower rates of descent ($\bar{V} > -1.5$) it generally over-estimates, with only a small error. At higher rates of descent ($\bar{V} < -2.0$), RVM underestimates the inflow compared to experimental data. Nevertheless, VRS is not expected to occur at those rates of descent, making this error of limited practical relevance in determining the bounds of VRS.

With the inflow model and super-positioned addition due to the vortex rings known, BET can be used to determine the required torque and resulting thrust of the rotor (Glauert 1926). XFoil (Drela 1989) is used to determine airfoil data for a range of angles of attack, Reynolds numbers and Mach numbers. An interpolation is performed on this data. Lift and drag values for the 2D airfoil can be requested by the blade element model, and are returned in a fraction of the computational time XFoil would take. This is advantageous for the large amount of requests during larger simulations with the highly discretized rotors, as XFoil takes a considerable amount of time to finish a request.

Nevertheless, an overly large discretization is superfluous and may still cause overly lengthy computational times. Instead, the minimal number of radial and azimuthal segments is to be determined that gives acceptable results; below approximately 0.05%. Figure 3.6 shows the relative error of the thrust coefficient computed using BET, for increasing resolution. For the radial resolution NR (Figure 3.6a), the rotor was analyzed in hover, negating any azimuthal influence. The figures show that the error (compared to an overly large resolution) indeed reduces with increasing resolution, dropping from $> 10\%$ at $NR = 10$ to below one percent at approximately $NR = 115$. $NR = 125$ is chosen as an acceptable point while still minimizing computational effort. Using this radial resolution, the azimuthal resolution $N\Psi$ is varied at an arbitrary forward speed (Figure 3.6b). The behavior of the error is slightly more sporadic, but still shows the same general trend of decreasing error with increasing resolution. Furthermore, the error diminishes more quickly compared to the radial resolution. As a result, an azimuthal resolution of 18 is chosen, reducing the error to below 0.01%.

[2] Data was extracted by digitizing a plot and can carry errors.

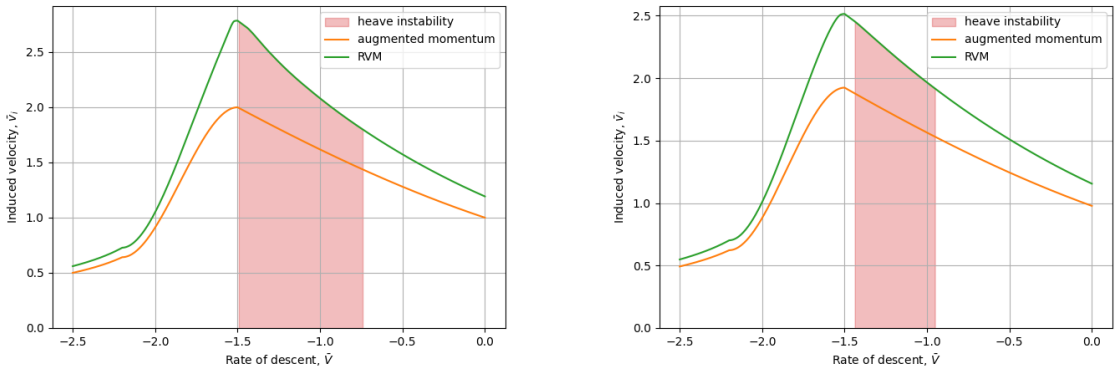


(a) Radial **(b)** Azimuthal

Figure 3.6: Error due to blade element discretization

3.3. VRS Boundaries Determination

The model (section 3.1 and section 3.2) models a rotor in descent, including VRS. However, this does not immediately determines the bounds of VRS, i.e. the extreme rates of descent and forward speed for which VRS occurs. Various criteria to detect VRS exist are discussed in section 2.6. Foremost, simply looking at the average inflow over the rotor disc allows for the heave instability criteria to be applied (subsection 2.1.2). The inflow from momentum theory is plotted for both axial and oblique (with forward speed) descent, along with the corrected inflow using RVM.



(a) Axial descent ($\bar{V} = 0$) **(b)** Oblique descent ($\bar{V} = 0.3$)

Figure 3.7: Heave instability with RVM

Under the RVM data line (Figure 3.7a) an area is shaded red where $\frac{\delta v_i}{\delta V} \leq -1$ applies; the heave instability. The same model is applied to forward flight. Here, the vortex rings have a horizontal offset, which decreases the amount of inflow they oppose onto the rotor. This is shown as a smaller interval at which VRS is expected, which corresponds with the concept of the vortex structure being swept away from the rotor by the forward airspeed (Figure 3.7b).

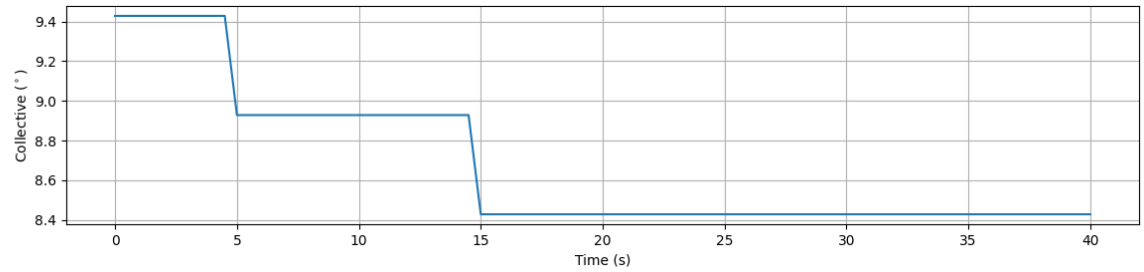
The detection of VRS using heave-instability is rather elementary and does not allow for local effects to be analyzed, such as the varying inflow, blade twist, chord or blade profile. BET (section 3.2) does allow for these effects to be taken into account. Figure 3.8 shows the significance of the local effects, as the erosion-pattern clearly shows a varying angle of attack over the blade. Though VRS is mainly an aerodynamic phenomenon and not necessarily rooted in flight-dynamics, such a model shows clear signs of VRS. The model rotor is trimmed in hover, after which a series of collective commands initiate and sustain a descent. The rotor can only move and accelerate downward or upward and does not tilt. If the rotor has a forward speed, it is constant. Furthermore, the rotor is continuously trimmed in pitch and roll, even after a collective drop is commanded. The inputs required to trim the rotor are found using Brents method (Brent 1973), which is robust and does not require the computation of derivatives of control responses.



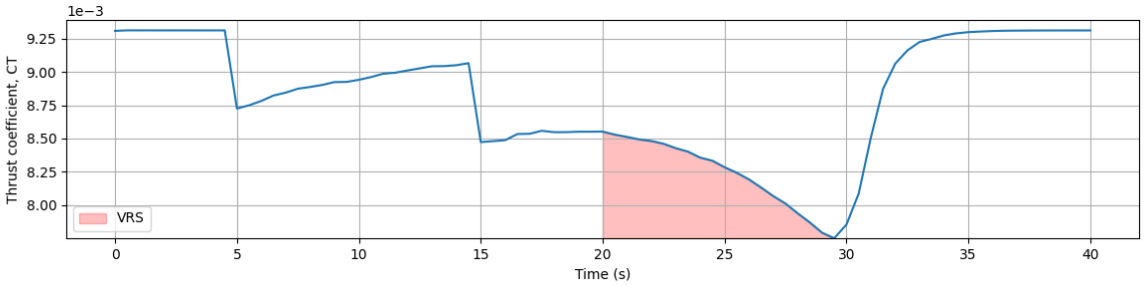
Figure 3.8: Erosion on a RNLASF CH-47F Chinook aft rotor blade (author's photograph)

The results of this simulation, with a run-time of 50 seconds at one second intervals, are shown in Figure 3.9. The rotor is in axial descent. A decrease in thrust is seen with the first collective drop after 5 seconds (Figure 3.9b), after which the helicopter starts descending (Figure 3.9c). With the increasing rate of descent, the rotor experiences an increasing upflow. At the same collective setting, this increases the angle of attack everywhere on the rotor blade. In turn, this increases the thrust, slowing the acceleration until the system stabilizes at a certain rate of descent. In this simulation, it is seen how the thrust starts to recover, but a new collective decrease is commanded.

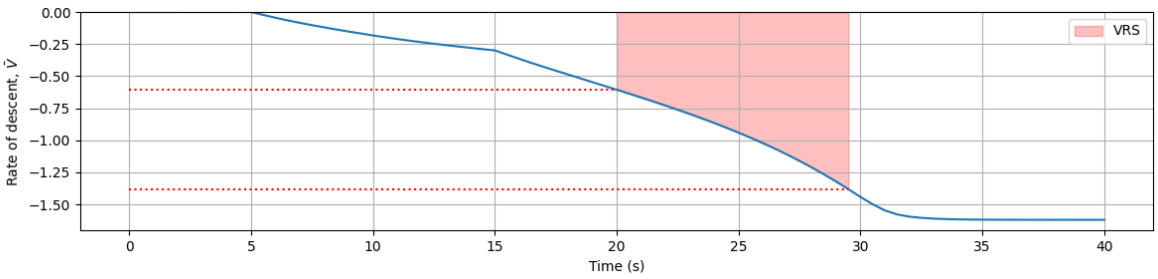
After the second collective decrease at 15 seconds, it is seen that the recovery of a stable descent slows down. After 20 seconds, the system fails to recover to the thrust level that sustains the helicopters weight. Instead of an increase in rate of descent leading to more thrust, the relation is now the opposite way around. As a result, the rate of descent increases further, and the downwards acceleration is faster. This phenomenon is still the heave-instability as before, but now local effects of the inflow and rotor geometry are taken into account. VRS is present where the thrust is decreasing, excluding when the decrease is a direct effect of the commanded collective decrease. The red-shaded area marks the expected VRS (Figure 3.9). After 29.5 seconds, the thrust recovers, marking the end of VRS. It is important to note the helicopter stabilizes to a constant rate of descent, but does not stop descending. This stabilization is a direct effect of the inflow through the rotor decreasing after the VRS region (section 3.2).



(a) Collective profile



(b) Thrust



(c) Descent speed

Figure 3.9: Flight dynamics based model of a rotor in descent

A major implication of this time based method is that the rotor is not necessarily trimmed at any time, except at the start or when the rotor settles at a certain rate of descent. This varying thrust also influences the inflow through the rotor, which influences the thrust computed with BET. As a result, each time-step requires an iterative approach, converging to a consistent inflow and thrust. Even when feeding the solution of the previous point in time of the simulation as a starting point for the next, the computational effort required is significantly increased. Alternatively, instead of a model rooted in flight-dynamics, a certain rate of descent can be imposed, after which the rotor is trimmed to deliver 1G of thrust. Evaluating a range of rates of descent, in which VRS is likely to occur, the full descent of the rotor can still be analyzed. The 'falling through' (heave-instability) of the rotor as a method to find VRS is no longer valid as the rotor thrust stays constant over time. Another criteria to determine the bounds of VRS is to be used.

Instead, once the collective required to trim the rotor for a range of rates of decent is determined, the bifurcation criterion (Prasad et al. 2004) can be applied. The collective required is plotted against the rate of descent (Figure 3.10). In a normal flight regime (between hover and the start of VRS), a higher rate of descent would require a lower collective setting, as the upflow due to the descent increases the angle of attack over the rotor blades. The additional thrust produced by this increased angle of attack is to be negated by decreasing the collective setting, as the rotor is to stay trimmed. However, in VRS an increase in rate of descent causes an increase of the inflow, more so than the upflow due to the descent negates. This is analogous to the heave instability. The normal situation (with rates of descent lower than those at which VRS is found) is marked by a positive slope. It is seen how there is a

reversal; a section with a negative slope shaded red (Figure 3.10). This is indicative of a thrust control reversal and is an indication of VRS. This method is preferred over the method of heave-instability as the method of bifurcation allows for local aerodynamic effects to be considered. Furthermore, bifurcation is preferred over the method rooted in flight-dynamics, as it is less computationally expensive. The rotor is also trimmed at any time, giving consistency. The bound corresponding to a lower rate of descent ($\bar{V} = -0.51$) is referred to as entry. The bound at the higher rate of descent ($\bar{V} = -1.48$) is referred to as the exit. This is consistent with a helicopter starting in hover, increasing its rate of descent to find VRS. In principle a helicopter can also enter VRS from the exit point, but the naming convention is kept.

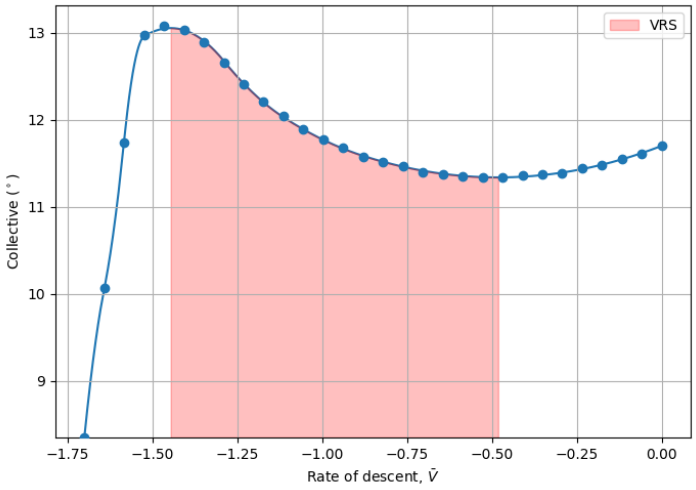


Figure 3.10: Collective profile for a trimmed rotor in axial descent

3.4. Tandem-Rotor Interference Model

A multi-rotor system, specifically a tandem-configuration as the Boeing CH-47 Chinook is to be analyzed. The analysis required is similar as for the single-rotor, albeit that the interference between the intermeshing rotors has to be included. Any two (or more) rotors within some proximity have aerodynamic interference, as the rotor wake, including the vortex structure shed by the rotors at the tip, have a flow-field around them. A smaller separation between the rotors results in more interference. In VRS, the vortex structure stays around the rotor for a prolonged time (chapter 2), such that the influence of this structure becomes even more important. For a Chinook helicopter, both rotors are closely positioned and have a radial overlap of $> 70\%$ [3], such that interference is expected to be even more influential compared to a set of non-overlapping rotors.

Specifically in VRS, as the vortex structure sits around either rotor, the other rotor is hypothesized to sweep through this structure, such that a pronounced VRS may never be reached before it is swept away. For a co-axial rotor, the bundling of vortices into a torus-shaped structure is observed, but it is to be noted how in such a configuration, released vortex 'rings' (or rather the helical structure) are still concentric between both rotors (Makeev et al. 2022). However, for a tandem-rotor thrust-fluctuations as seen in single-rotor VRS are also present (Washizu et al. 1966), indicating that they are not resistant to VRS. As a result, RVM as described in section 3.1 is still used, with both rotors shedding their own vortex rings.

As discussed in section 2.5, in order to simulate rotor-rotor interference, the wake must be modeled. With RVM, the wake (or rather the vorticity carried by the wake) is readily present, and the influence of this wake on the other rotor is easily incorporated within the blade element framework. However, this approach models interference between wakes and rotors, not wakes themselves. This wake-wake interference is significant (Brown 2024). The influence of a vortex ring at any distance is analytically

[3] I.e. the spacing between both rotors is less than 1.3 times the rotor radius.

described by Castles and De Leeuw (1953), as readily used for the single rotor analysis (Appendix E). With a Chinook, the rotors are tilted with respect to each other (Figure 3.11). With increasing forward speed, the tip path plane (TPP) of the rotors tilt forward even more to ensure that the rather large fuselage of the Chinook stays mostly aligned with the direction of flight to minimize parasitic drag. In any case, even in hover the rotors are tilted, with the front rotor tilted 7.8° with respect to the fuselage, and the aft rotor 0.75° (United States Army Warfighting Center 2006). This tilt stays constant below $60kts$, and can thus stay constant within the scope of this VRS simulation.

LCT system

The CH-47 uses a longitudinal cyclic trim (LCT) system, which changes the longitudinal cyclic setting of the rotor disks depending on the forward flight velocity. Even on the ground, the rotors are tilted forward with the front rotor tilted 9° with respect to the fuselage, and the aft rotor 4°. This allows the Chinook to produce forward thrust to taxi. The moment the helicopter lifts off, the rotors are tilted back, to allow the helicopter to hover without excessive pitch. This is named retraction of the rotors.

A conventional helicopter, once the cyclic control is pushed forward, starts to accelerate. The disc is tilted forward as the cyclic pitch is applied and forward thrust is produced. A Chinook pitches forward by using differential pitch between both rotors, with the aft rotor producing more thrust. This tilts the rotors and the fuselage as a whole, such that more forward thrust is produced.

Once the Chinook starts to accelerate, the large, tilted fuselage starts to produce excessive parasitic drag. For forward speeds of $60kts$ (when the front and aft rotor are tilted 7.8° and 0.75°) and higher, the LCT tilts the rotors forward, allowing the fuselage to return to a more horizontal orientation. At a forward speed of $150kts$, the rotors are fully extended to 13° and 8°. Beyond this speed, a further tilting of the disc is only achieved by tilting the Chinook, including its fuselage, as a whole. (United States Army Warfighting Center 2006)



Figure 3.11: RNLASF CH-47F Chinook in hover or slow forward flight. Image used with photographer permission © Ludo Mennes, Northern Skies Aviation

Assuming that both rotors have to produce equal thrust [4], the Chinook fuselage itself tilts 4.275° backwards in hover. Figure 3.12 shows an overview of the rings and the rest of the wake for the Chinook in hover. Without a horizontal velocity, the wakes propagate downstream perpendicular to the rotors, and so do the vortex rings. The TPPs of the rotors are no longer aligned with the direction of forward flight. Therefore, any forward speed or rate of descent of the Chinook as a whole introduces both a forward speed along the TPP and a rate of descent/ascent normal to the TPP at each rotor. A simple transformation of coordinates ensures that the velocities of the Chinook as a whole are correctly

[4] This is not generally true and depends on the weight and balance of the Chinook.

translated to the local velocities of each rotor. The only difference with respect to the single-rotor case, is the tilt of the vortex rings emitted by the other rotor, which are not only translated, but also slightly rotated. Only the inflow due to a vortex ring normal to the plane in which said ring is situated, is described. With not the entire flow-field known, this introduces a small error. As the tilt between one rotor and the rings of the other rotor is only 7°, this error is accepted.

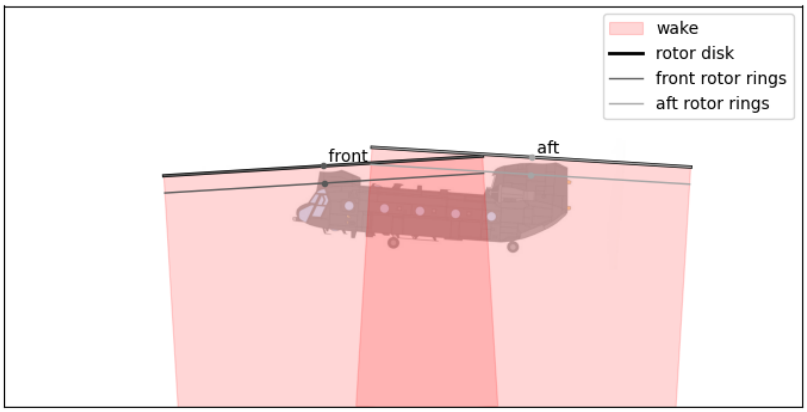


Figure 3.12: Overview of RVM components for the Chinook in hover

The vortex rings of each rotor interferes with the other rotor. However, a wake does not only consist of tip vortices (though they are the dominating part of the wake in a VRS simulation). The induced velocity generated by one rotor can be super-positioned upon the other, at least for the overlapping section (Sheen et al. 2023). This has not been applied to RVM before, as solely non-overlapping multi-rotor configurations were analyzed. For a Chinook (Figure 3.11 and Figure 3.12), the intermeshing part of the rotors sweep through each-other as they have a 70% radial overlap, such that the downwash generated by the aft rotor interferes with the front one and vice versa. This simple super-positioning of inflow ignores mutual effects on the inflow. As an example, the added inflow of one rotor onto the other rotor decreases the local angle of attack of said rotor. This decreases the local thrust and ultimately decreasing the local inflow, as the inflow depends on the thrust of the rotor. Hence, the sum of the rotors own inflow and the superimposed correction that accounts for interference, is an overestimation of the actual local inflow.

The mutually imposed inflow can simply be corrected by a factor. Chen et al. (2019) analyzed a tandem-rotor. Each rotor has a 26.8% overlap, and a total additional induced power of 15% is observed. The most simple method of analyzing required power by a helicopter is with momentum theory. The required induced power P_{ind} is equal to the produced thrust T times the induced velocity v_i:

$$P_{ind} = Tv_i \tag{3.6}$$

Equation 3.6 shows that the induced power scales with the induced velocity over the rotor. The 26.8% overlap should thus result in a 26.8% increase of inflow averaged over the rotor. Only a 15% increase in thrust was observed however, and thus a mutual inflow factor k_{mi} of 15/26.8 = 56% is used. This simpler method does not require the implementation of a more complex inflow model and is thus preferred. In the scope of this thesis, this specific component of the inflow is referred to as mutual inflow to distinct between this component and that of the mutual vortex rings.

With the simulation of the tandem-rotor discussed, it is to be utilized to find the VRS boundaries of both rotors. Bifurcation is to be applied to the tandem-rotor as well, as was done for the single rotor (section 3.3). The relation between collective and rate of descent for the aft rotor is shown for a forward speed of $\bar{V}_x = 0$ (Figure 3.13), with the front rotor showing a similar relation. Although the graph looks

similar to Figure 3.10, a dip is shown in the required collective around $\bar{V} = -1.5$. At this rate of descent, the velocity of the wake compared to the rotor is diminished, such that the mutual inflow becomes almost zero. With the lesser inflow, the required collective is smaller. This is merely an effect of the chosen method to model rotor-rotor interference for a set of overlapping rotors. It does not mark an end to VRS, rather the contrary. The collective required for a certain rate of descent (Figure 3.13) is readily interpolated between $\bar{V}$ values. This limits the amount of computations required, while allowing for any rate of descent to be marked as the bound of VRS, instead of only the pre-determined discrete $\bar{V}$ values that were analyzed. This interpolation ignores the dips around $\bar{V}_{peak}$ (= −1.5), allowing for an exit bound to be determined. Similarly, this relation is interpolated between the discrete $\bar{V}_x$ samples, allowing for the last $\bar{V}_x$ at which VRS is found to be determined.

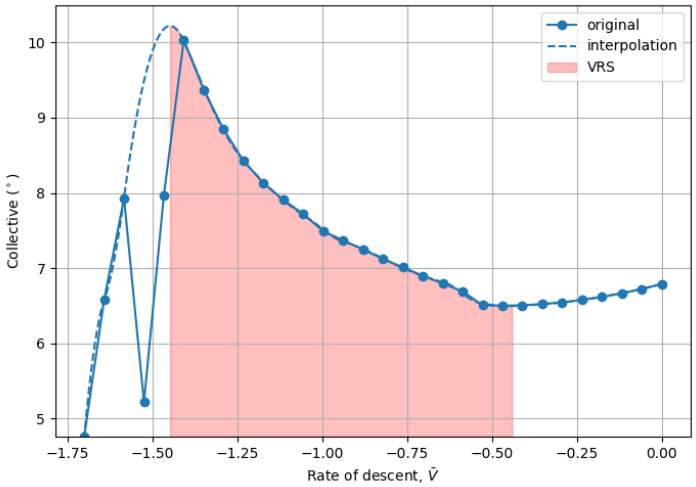


Figure 3.13: Bifurcation applied to aft rotor ($\bar{V}_x = 0.5$)

3.5. Assumptions

Next to assumptions that are inherent to RVM or other models used, a number of assumptions were made in this thesis. These assumptions are listed here for clarity.

3.5.1. Rotor and Blade Modeling

- Blade flapping and lead–lag motion are not modeled. Although blade flapping is characterized as fluctuating and can serve as an indicator of VRS onset (Leishman et al. 2002), the dominant mechanism underlying VRS is the wake of the rotor. Accurately resolving the unsteady rotor loads is therefore not necessarily advantageous for determining the VRS boundary.
- Rotor TPP tilt is not modeled, apart from the tilt due the described LCT (section 3.4).
- Effects of the Chinook fuselage are ignored.

3.5.2. Tandem-Rotor Interference Model

- Only the interference between one rotor and the wake of the other rotor is modeled. Wake-wake interaction between the two rotors' wakes is not.
- The velocity a ring from one rotor induces on the other rotor is calculated in a plane normal to this ring. The small error from the 7° tilt between both rotors and thus rings is ignored.

4

Deterministic VRS boundaries

The methodology described in chapter 3 is now applied to a single- and multi-rotor helicopter. The single rotor is simply one of the two identical chinook rotors in isolation, carrying half the weight of the full Chinook. The relevant parameters are provided in Appendix B.

4.1. Single Rotor VRS Bound

The RVM method as described in chapter 3 is applicable to find VRS boundaries in both axial and oblique descent. The analysis is performed at a range of forward speeds ($0 < \bar{V}_X < 0.7$), after which the entry and exit points are plotted. The bound of VRS is drawn by connecting these points and thus expressed in terms of rate of descent $\bar{V}$ and forward speed $\bar{V}_x$ (Figure 4.1). The upper section is referred to as VRS entry, the lower part is referred to as the exit. The right-most bound, the last $\bar{V}_x$ at which VRS is found, will be referred to as the last $\bar{V}_x$. In order to determine this point, the relation between collective and rate of descent is interpolated between actual computed values of $\bar{V}_x$, marked by the round blue and orange markers.

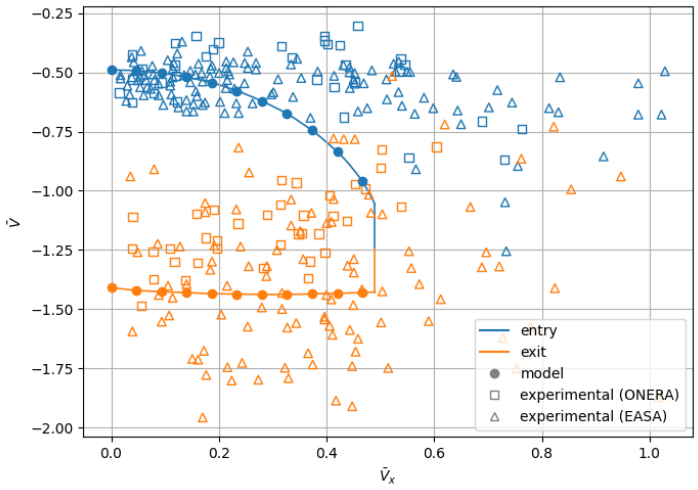


Figure 4.1: Predicted VRS entry and exit boundaries compared with ONERA and EASA experimental data (Taghizad et al. 2002; Binet and Basset 2025)

Figure 4.1 shows the VRS bounds computed with the use of RVM, compared to experimental data[1], which is gathered by ONERA (marked with squares) and EASA (marked with triangles) (Taghizad

[1]Data was extracted by digitizing a plot and can carry errors. Furthermore, the data is normalized with a singular average weight during the flight-tests

et al. 2002; Binet and Basset 2025). In Appendix C, the same plots are given with just one set of data per plot, allowing for the bound to be compared to each set of data seperately. For lower forward speeds ($\bar{V}_x < 0.2$), the predicted bound aligns with experimental data. Especially for the entry into VRS, marked by the blue points, the predicted bound aligns with the average of experimental data. For the exit, the bound determined with the RVM model predicts VRS to exist for higher rates of descent than ONERA experimental data suggests. EASA data correlates better, but its scatter is very high. At higher forward speeds (approximately $\bar{V}_x > 0.2$), the prediction is less accurate, with the model predicting VRS to occur at higher rates of descent. The experimental data shows VRS at forward speeds up to $\bar{V}_x = 1.0$, while the model predicts VRS ceases to exist at forward speeds over approximately $\bar{V}_x = 0.5$.

The discrepancies between model predictions and experimental data are of various origins. VRS predicted to exist at higher rates of descent, especially at higher forward speeds, is likely due to limitations of the RVM methodology. Because RVM uses experimental data to define the peak of VRS at $\bar{V} = -1.5$, the predicted boundary is partly biased toward this value. Furthermore, RVM is inherently inaccurate for a more developed VRS, as the wake becomes less structured (section 3.1). The under-prediction of the forward speed at which VRS ceases to exist, can be attributed to RVM as well. The skewed wake with the vortex rings keeping their orientation can be seen as an overly crude approximation of a rotor wake in oblique descent (subsection 2.3.1). Nevertheless, though this prediction is less consistent with the experimental flight-test data, this data is not necessarily perfectly applicable. The data was gathered by noting the rate of descent at which a sudden increase in this rate of descent occurred. VRS is accompanied by many different symptoms (subsection 2.1.2), which do not necessarily occur at the same rate of descent. The point at which the increase in rate of descent occurs could simply not align with the point at which the bifurcation criterion is met (Binet and Basset 2025). Furthermore, the data shows some abnormalities like VRS entry occurring after exit around $\bar{V}_x = 0.55$. The ONERA and EASA data also correlate poorly between themselves, even though both sets were gathered using the same criteria and even the same or similar helicopters. This is especially noticeable at the VRS exit, where the data from EASA show a larger spread. These considerations decrease the quality of the data. Analytically derived bounds from literature predict VRS ceasing to exist at ranging values of $\bar{V}_x$ as well (Binet and Basset 2022). In conclusion, the imperfect match between model prediction and experimental data does not invalidate the model, although the model is more suited to predict VRS entry at lower forward speeds.

4.2. Tandem-Rotor VRS Bound

Similarly to the results from section 4.1, the results for the tandem-rotor are displayed, using the methodology as described in chapter 3, specifically section 3.4. The tandem-rotor results are compared with the isolated single-rotor case, which is one of two identical Chinook rotors, to identify the consequences of aerodynamic rotor-rotor interference. The rotors of the tandem-rotor show interference, as they differ from the bound of the single rotor (Figure 4.2).

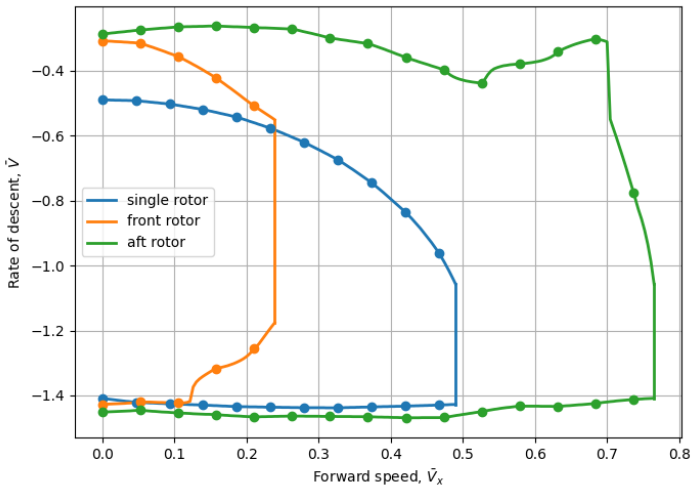


Figure 4.2: Tandem and single rotor VRS bounds

The primary result is that rotor-rotor interference changes not only the position or span of the VRS boundary, but also the boundaries overall shape. In axial descent ($\bar{V}_x = 0$), the bounds of VRS are wider (specifically entry into VRS), for both the front and aft rotor. This is caused by the extra rings and overlapping rotors imposing more inflow through the overlapping part of the rotors. As a forward speed is introduced, the wake skews as seen in Figure 3.2. Both sets of vortex rings move back relative to both rotors. As the rings shed by the aft rotor move back, a smaller section of the front rotor experiences added inflow through the rotor. Outside the circumference of the vortex ring, the front rotor even experiences upflow from below. This decrease in additional inflow tightens the bounds of VRS. Additionally, VRS ceases to occur relatively quick at moderate forward speeds. In contrast, the aft rotor shows VRS to occur until fairly high forward speed, and shows generally wider bounds in terms of $\bar{V}$. As the rings shed by the front rotor move towards the aft rotor, the inflow through the rotor at a higher range of forward speeds is increased. This makes the aft rotor more prone to VRS at a larger range of forward speeds and rates of descent. Additionally, this asymmetry between both rotors makes the Chinook more prone to uncommanded pitching, a potentially dangerous phenomenon. Although no experimental data is available for the Chinook, the finding that tandem-rotors are more prone to VRS (especially the aft rotor) is consistent with the findings of Brown (2024) with a higher fidelity model.

The additional mutual inflow through both rotors because of the overlap (section 3.4) also results in the VRS bounds for the tandem-rotor being wider than for the single rotor, in terms of $\bar{V}$. However, the skew of the wake does not generally expand this influence to further forward speeds. Neither rotor (their tip path plane) is positioned significantly above the other (Figure 3.12). Instead, the effect stems from the inflow being non-uniform for forward flight. As a rotor flies forward, the inflow at the rear of the rotor increases compared to the front of the rotor. The aft rotor overlaps with the section of the front rotor that imposes this additional inflow, such that the aft rotor has even more inflow through this overlapping section. In a different design, where one of the rotors would be positioned more above the other, a less significant interference would be seen. The skewing wake would have a less significant effect, as the intersecting region is smaller.

Although the bounds of VRS generally tighten with forward speed, a certain reversal is seen around $\bar{V}_x = 0.5$ for the aft rotor (Figure 4.2). The added inflow the front rotor imposes onto the aft rotor, is a more dominant effect than the vortex rings being blown away by the forward speed. This behavior is not limited to $\bar{V}_x > 0.5$. At lower forward speeds, the VRS entry bound narrows less quickly compared to the single rotor. On the contrary, the front rotor shows a faster decrease. The value $\bar{V}_x = 0.5$ should therefore be interpreted as a transition point rather than a strict threshold. At this forward speed, the reduction in vortex ring interaction due to wake convection becomes comparable to the increase in mutual inflow between the rotors.

These deterministic simulations demonstrate that rotor-rotor interference substantially modifies the VRS boundaries of a tandem-rotor helicopter. The mechanism governing this modification changes with forward speed, with mutual inflow becoming increasingly dominant relative to the direct influence of the vortex rings. As a result, the VRS bound for the aft rotor even widens after $\bar{V}_x = 0.5$. These observations form the basis for the uncertainty analysis in the next chapter.

5

Uncertainty Quantification

The chosen RVM model (section 3.1) oversimplifies the wake in VRS significantly, missing major characteristics of the phenomenon, including the interference between vortex rings. This interference results in a less organized vortex structure than RVM proposes. Furthermore, semi-empirical or even analytically derived values such as $\bar{V}_{peak}$ carry uncertainty. These uncertainties are epistemic uncertainties (section 2.7). By evaluating the model while altering uncertainty parameters, the uncertainty of the model can be quantified. Latin hypercube sampling (LHS, sampling based) is used, which is more efficient than Monte Carlo sampling (MCS) (subsection 2.7.1). Polynomial chaos expansion (PCE, surrogate based) is used to see if a smaller amount of samples can reproduce these results. This surrogate model will also show the effects the various uncertainty parameters have on the bounds.

5.1. Computational Cost Reduction

As uncertainty quantification (UQ) requires numerous model evaluations, computational efficiency becomes a prerequisite rather than a convenience. Considerable effort has been devoted to reduce the computational cost. A lower fidelity model was selected and results are interpolated (chapter 3), in order to keep it feasible to evaluate the model repeatedly. The results from chapter 4 were generated while trimming the rotor to produce 1G of thrust, and no pitching- or rolling-moments. This requires repeated re-evaluations of the modeled rotor. Solely trimming the collective, which is essential to apply the method of bifurcation, results in significant time savings. The inflow model ignores the resulting moments of the rotor as well, as otherwise repeated evaluations are needed regardless.

The error introduced by leaving the rotor untrimmed in rolling-and pitching moments (Figure 5.1) is zero in axial descent ($\bar{V}_x = 0$), which is expected as the single rotor's wake is axisymmetric.With the introduction of forward speed, this error starts to increase. This is expected, as there is a dissymmetry of lift and a varying inflow, both typical for rotors in forward flight. The error stays below 2% until $\bar{V}_x = 0.47$, where it goes up to 7%.

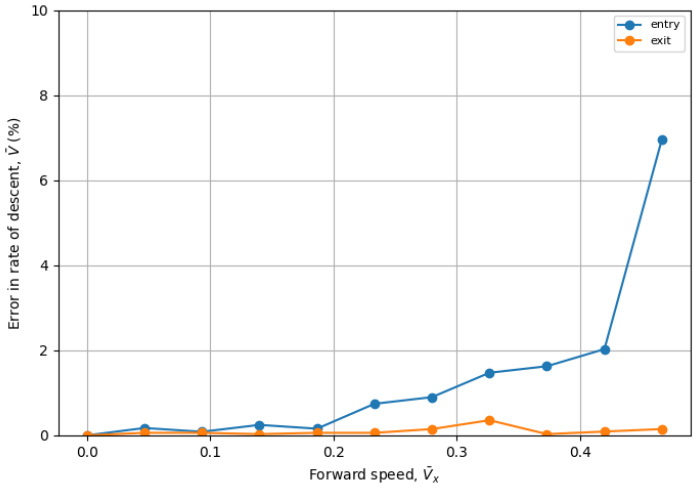
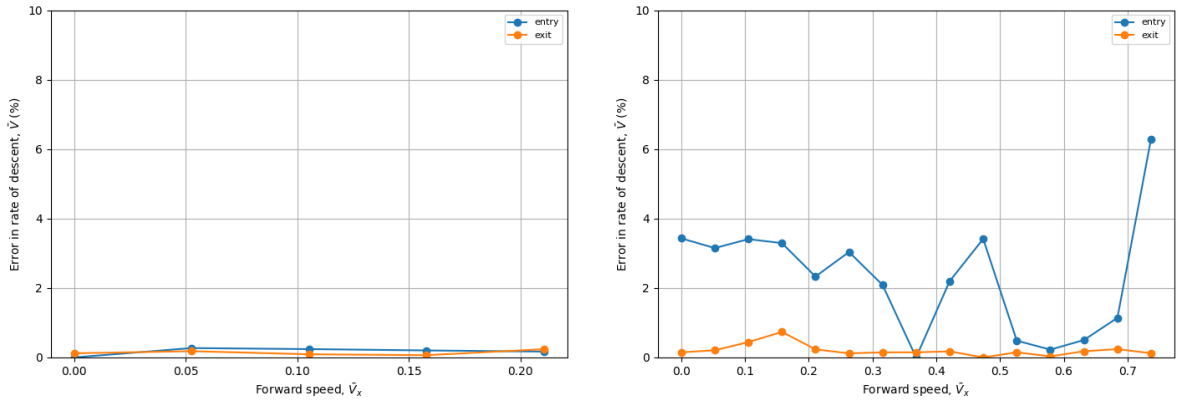


Figure 5.1: Error introduced by neglecting moments

For the front rotor of the tandem configuration (Figure 5.2a), the error is close to zero, as VRS ceases to exist before higher forward speeds are reached (chapter 4). However, the aft rotor (Figure 5.2b) shows a higher error, also at lower forward speeds.



(a) Front rotor

(b) Aft rotor

Figure 5.2: Error due to ignorance of trim in tandem configuration

The cost in terms of inaccuracy are small compared to the time savings, which are 74% and 87% for the single- and tandem-rotor, respectively. Furthermore, an absolute error in the bound of VRS does not translate to a similar error in the uncertainty of said bound. Uncertainties in RVM stem from inaccuracies in the modeled wake and experimental data, not necessarily from leaving the rotor untrimmed. Hence, these errors are accepted, to keep the computational cost of a UQ limited.

5.2. uncertainty parameters

Design parameters like the amount of rotor blades per rotor have a significant influence on VRS modeled with RVM, as this influences the shedding interval of the vortex rings. However, design parameters are outside of the scope as the analysis focusses on model uncertainties. These uncertainties originate from experimental evidence where available, supplemented by engineering judgement.

Parameter	Parameter name	Type	Reference	standard deviation
Vortex ring strength	k_Γ	Factor	0.1333	5%
Vortex ring spacing	Δ_{ring}/R	Offset	0	0.02
VRS peak	$\bar{V}_{peak}$	Factor	-1.5	10%
Lift coefficient	C_L	Factor	-	5%
Drag coefficient	C_D	Factor	-	5%
Mutual inflow	k_{mi}	Factor	0.56	10%

Table 5.1: Variances of uncertainty parameters

The normally distributed parameters and their uncertainty are summarized in Table 5.1. k_Γ represents the strength of the vortex ring as shed by the rotor. It is determined by relating the strength of the vortex ring to the amount of air moved through this ring, instead of analyzing the vorticity distribution over the blade. This simplification introduces uncertainty and so does the use of experimental data ($v_{i_{peak}}$) to determine k_Γ (section 3.1). This $v_{i_{peak}}$ (remembering that peak refers to $\bar{V} = -1.5$) is shown in Figure 2.2, with a scatter between approximately $2.2 < \bar{v}_i < 2.8$ around $\bar{V} = -1.5$. A standard deviation of 5% is hence chosen, such that the majority of the normal distribution falls within this range. Likewise, $\bar{V}_{peak}$ shows a larger variation, and a standard deviation of 10% is hence chosen.

Δ_{ring} signifies an offset to the rings, with which both rings are moved upwards, relative to the rotor radius. To allow the rings to even jump over the rotor, an offset is added instead of a multiplication factor, which would just compress the structure. Figure 5.3 shows the vortex structure around a rotor in the peak of VRS (QinetiQ 2024). The chaos of the structure is apparent. However, as a measurement of the variation in the vortex structure for the exact same conditions was not found in literature, the uncertainty is therefore estimated. A standard deviation of 2% of the rotor radius is chosen. This may not seem like a large number compared to the chaos of the wake in VRS. However, the spacing between rings is the largest in hover, where the spacing is 10.7% of the rotor radius. Thus, a 2% variation is relatively large. As the spacing decreases with a rate of descent, this variation becomes more significant.

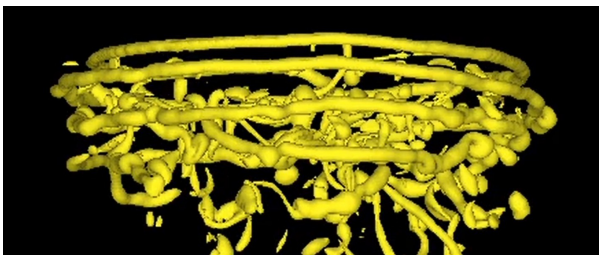


Figure 5.3: Vortex structure of a rotor deep in VRS (QinetiQ 2024)

The lift- and drag-coefficient have a 5% standard deviation (Siva et al. 2011). The uncertainty of these aerodynamic coefficients comes from errors of Xfoil and the interpolation of these results, used to determine the aerodynamic coefficients (chapter 3). Furthermore, as the rotor is flown, its profile is altered due to erosion (Figure 3.8).

The determination of the mutual inflow (k_{mi}) was accompanied by a range of assumptions (section 3.4), introducing uncertainty. Though the principle of superimposing inflow between overlapping rotors has been applied in literature, no exact uncertainties were presented. An uncertainty distribution with a standard deviation of 10% is estimated. This reflects the uncertainty in the modeling approach rather than physical uncertainty.

5.3. LHS results

LHS is chosen over MCS to decrease the amount of samples needed for the UQ. The median and 95% certainty band of the VRS entry and exit show a clear stabilization with an increasing number of samples for $\bar{V}_x = 0$ for the single rotor (Figure 5.4). The relative change per sample steadily decreases, with >230 samples showing changes below 0.5%, with sporadic outliers such as the spike of >5% no longer being present. The width of the 95% certainty band converges somewhat slower than the median. 300 samples were computed, of which 298 produced a VRS bound. The two samples not producing VRS to occur is not an error, but is due to a more extreme combination of parameters at which VRS was simply not found. Other forward speeds have similar convergence behavior and are therefore omitted for brevity.

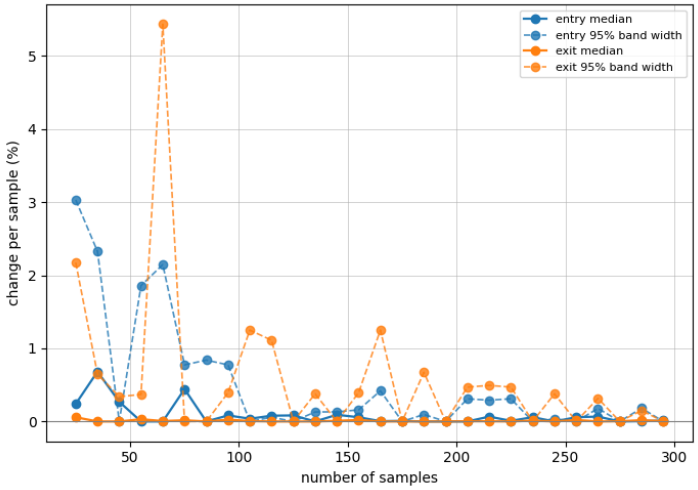


Figure 5.4: Convergence behavior of LHS sampling

All 298 determined VRS bounds are shown (at the $\bar{V}_x$ values for which they were directly evaluated) in Figure 5.5. The same distinctive shape as the singular bound (Figure 4.1) is seen. However, a significant scatter is seen around the entry point of VRS, for any forward speed. In hover, the scatter of the entry points is seen between $\bar{V} = -0.2$ and $\bar{V} = -1.2$, with most points sitting between $\bar{V} = -0.3$ and $\bar{V} = -0.7$. The $\bar{V}_x$ at which VRS ceases to exist also shows significant scatter (most points between $\bar{V}_x = 0.3$ and $\bar{V}_x = 0.6$). The points corresponding to VRS exit show some scatter, with points between $\bar{V} = -0.8$ and $\bar{V} = -1.55$. Compared to the singular bound, the scatter of the VRS exit is positioned more towards lower rates of descent, and the majority of points is bundled between $\bar{V} = -1.4$ and $\bar{V} = -1.55$. The lack of VRS bounds predicted at higher rates of descent is a direct effect of the inflow decreasing quickly for $\bar{V} < -1.5$ (Figure 3.5a). The bundling around $\bar{V} = -1.5$ is attributed to RVM selecting this as the most prominent part of VRS. The 10% standard deviation suggests 95% of samples should fall within a 20% range of $\bar{V} = -1.5$, but the majority of the predicted bounds fall within a 7% range. This is again attributed to the inflow peaking around $\bar{V} = -1.5$.

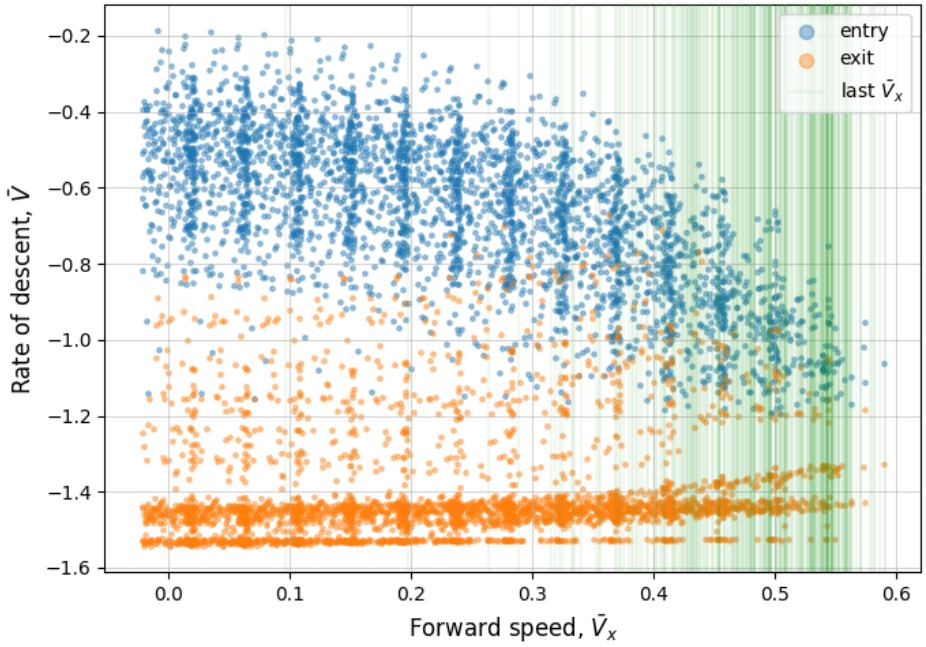


Figure 5.5: VRS bound samples with LHS

The scatter of points can be converted into a median and percentile certainty bands for the range of $\bar{V}_x$ values, giving a less cluttered graph. Figure 5.6 shows the 95% certainty band of the VRS bound for the single rotor, with the median bound in black. The plot is compared to experimental data from ONERA and EASA (Taghizad et al. 2002; Binet and Basset 2025), as was the singular bound (chapter 4), and Appendix C again shows the same plots with separate experimental data. Unfortunately, the limited amount of samples of the experimental data does not allow for an uncertainty bound to be drawn for a more direct comparison.

For lower forward speeds ($\bar{V}_x < 0.3$), the experimentally determined entry points fall well within the uncertainty bounds, although the simulated 95% uncertainty is larger. This aligns with the earlier observation that RVM is fairly accurate for single rotors at lower forward speeds. The ONERA experimental points of the VRS exit now show much better alignment with RVM too, in contrast to earlier observations (chapter 4). However, correlation to EASA experimental data is lower, with the uncertainty being significantly larger. Furthermore, for the orange band corresponding to VRS exit, the experimental points from ONERA correlate better with the model for somewhat higher forward speeds as well (until $\bar{V}_x = 0.4$). For the entry points RVM is less accurate at these higher forward speeds, aligning with earlier observations (chapter 4). Likewise, experimental data suggest VRS occurs until well outside the range predicted by RVM (shown in green, $\bar{V}_x < 0.6$), but the same limitations to the data as described in chapter 4 apply. The large resulting uncertainty of the VRS bound, and the fact that the uncertainty analysis suggest RVM may be a better model than deterministic results suggest, shows the value of a UQ.

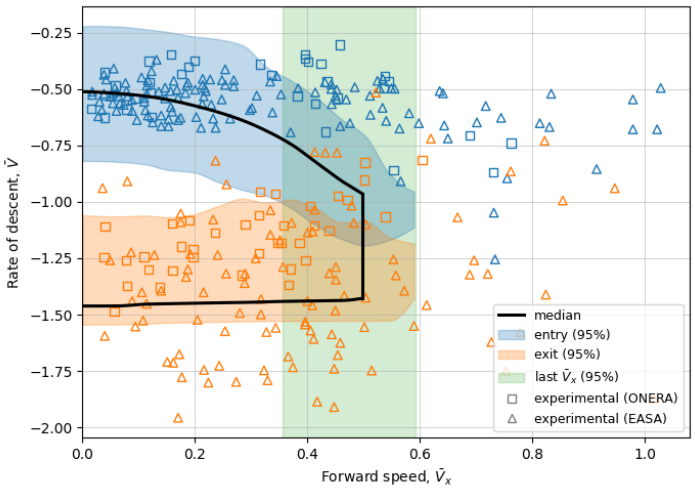
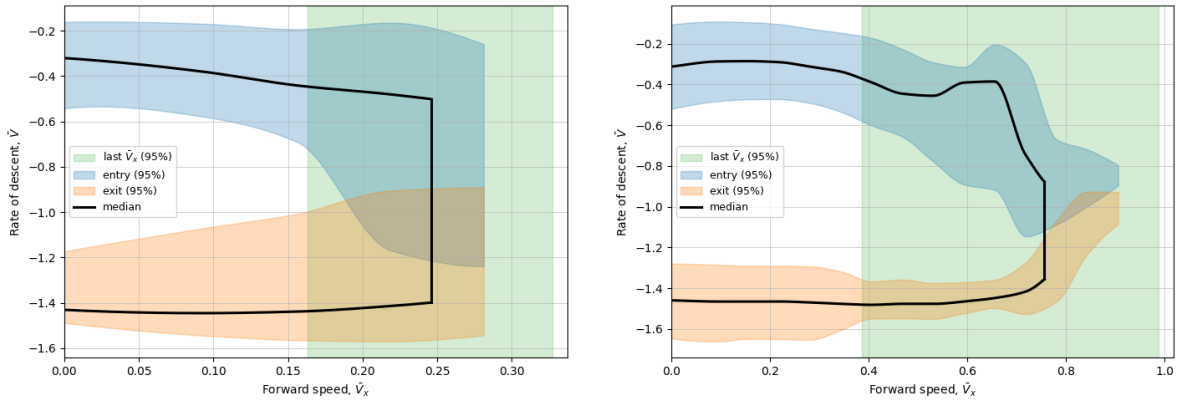


Figure 5.6: 95% certainty band of the VRS bound for a single rotor

300 samples are gathered for the tandem-rotor using LHS, for both the front rotor (Figure 5.7a) and aft rotor (Figure 5.7b). Similarly to the single rotor, after 230 points, both rotors showed convergence within 0.5% per sample for most forward speeds. However, at higher forward speeds samples are more scarce, such that the predicted uncertainty is less accurate.

The front rotor shows a smaller uncertainty around lower forward velocities ($\bar{V}_x < 0.2$), with the uncertainty increasing as $\bar{V}_x$ increases. The same is true for the aft rotor, with smaller uncertainties seen before $\bar{V}_x = 0.5$ for entry into VRS, and for all forward speeds for the exit. The uncertainty for the exit out of VRS for the aft rotor even decreases after $\bar{V}_x = 0.4$. The lower uncertainty for the tandem-rotor can be attributed to the mutual inflow being an influential mechanism in this tandem-configuration, apparently carrying less uncertainty. With the lack of validation data for the Chinook, it is unknown whether these effects are physical interference effects or merely exist in this simulation.



(a) Front rotor

(b) Aft rotor

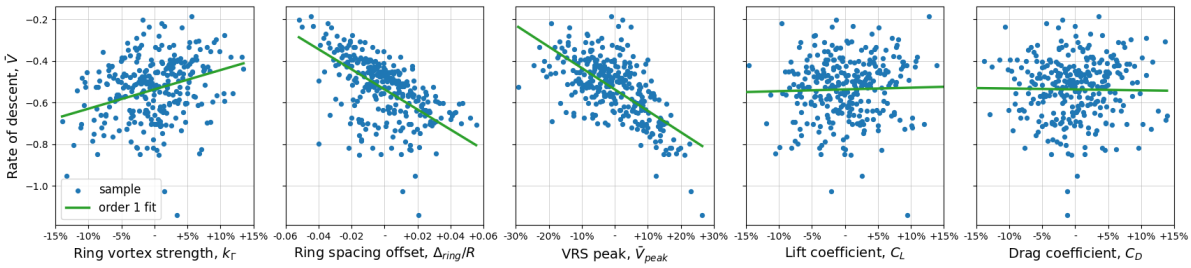
Figure 5.7: 95% certainty band of the tandem-rotor VRS bounds

5.4. PCE Results

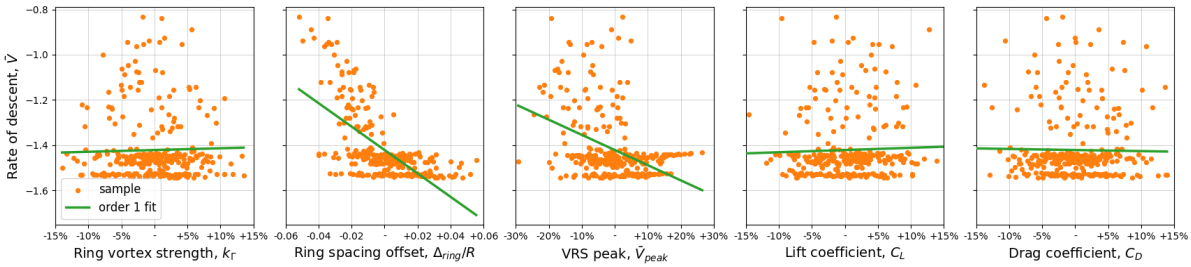
PCE is a potentially more computationally efficient method for UQ than LHS. Although PCE ultimately proved unsuitable for this implementation of RVM, the surrogate model provides valuable insight into the sensitivity of the uncertainty parameters. With PCE, a series of orthogonal polynomials is fit to the samples, relating the bounds of VRS to these uncertainty parameters. This surrogate

model can then be used to compute large amounts of samples at a fraction of the computational cost of a regular sample. Before the quality of this surrogate model is discussed, fitting the polynomials to the samples conveniently allows for the effect of the various uncertainty parameters to be discussed.

Figure 5.8 shows the training points (samples) around $\bar{V}_x = 0$, i.e. the first bin[1] of data. The vertical axis shows the VRS entry and exit bound, expressed in the rate of descent $\bar{V}$. The horizontal axis shows the variation in the uncertainty parameters. A first order polynomial fit is shown in green. Focusing on the entry points (Figure 5.8a), the relations between the uncertainty parameters and VRS entry points are clearly seen. An increase in the vortex ring strength (k_Γ) causes VRS to occur at a lower rate of descent, as expected. Likewise, shifting the rings up (a negative Δ_{ring}) or decreasing $\bar{V}_{peak}$ causes VRS to occur at a lower rate of descent. Although VRS is an aerodynamic phenomenon, it is apparent that the variation in C_L and C_D show little to no influence on the bounds of VRS, as seen by the horizontal fit. The vortex ring's strength in RVM is determined by the amount of air moved through said vortex ring (chapter 3). Therefor, it is not determined by the loading of the rotor blade and thus C_L or C_D values over the blade. Furthermore, VRS being an aerodynamic phenomenon mostly relates to the wake and not directly to the rotor, which is deemed less significant in VRS (subsection 2.1.2). The low dependency on these aerodynamic characteristics of the blade-profile are thus not unreasonable. It also confirms that the selection of another airfoil, as the actual Chinook airfoil is unknown (Appendix B), does not have a significant influence on the results.



(a) VRS entry



(b) VRS exit

Figure 5.8: Sample scatter ($\bar{V}_x = 0$) with first order polynomial fit

The same trends between the uncertainty parameters and VRS bounds are observed for the exit points (Figure 5.8b), although the strength of the vortex rings shows to be less influential, indicated by the horizontal fitted line. This is expected as the vertical spacing between the inflow and the ring show a very strong relation when the spacing is small (Castles and Gray 1951). As the rings are close to the rotor, a small difference in their strength does not influence the inflow enough to alter the prediction of the VRS exit point. The spacing of the vortex rings to the rotor is the dominant factor, and this is confirmed by the steeper gradient of the polynomial fit relating to Δ_{ring}.

The plot showing the relation between the VRS exit and $\bar{V}_{peak}$ shows a lack of scatter for higher values

[1] A range of forward speeds in which the samples are grouped. The given $\bar{V}_x$ values are the centers of the bins.

of $\bar{V}_{peak}$. This implies that only for a lower value of $\bar{V}_{peak}$, the other uncertainty parameters vary the bound. For higher values of $\bar{V}_{peak}$, the simulation never 'breaks free' from the prescribed peak. Such interactions between these parameters suggest that a higher-order polynomial as a basis for the PCE is required. A higher order does however require more samples, as the polynomial function that is to be fit has more degrees of freedom to be constrained. Furthermore, using more samples gives a better fit, as using the mathematical minimum amount of required samples often still introduces errors. The absolute mathematical minimum N_{PCE}, expressed in order p and amount of uncertainty parameters d is given by Equation 5.1. However, twice the amount of samples is recommended (Hosder et al. 2007).

$$N_{PCE} = \binom{d+p}{p} = \frac{(d+p)!}{d!\,p!} \tag{5.1}$$

For a first order PCE with 5 uncertainty parameters, $N_{PCE} = 6$, but for a second order fit this increases to $N_{PCE} = 21$. Figure 5.9 shows the amount of samples per bin. It is seen how the last bin that still holds valid points that show VRS, has enough points to be fit with a first order function. However, more points are required for a second order fit. Bins can be grouped to hold more points per bin, but this decreases the resolution in $\bar{V}_x$ direction. Instead, if a bin shows too little points, it is simply ignored. This is a limitation of PCE, but the uncertainty as determined with a more simple sampling-based method (LHS) is also more error-prone as lesser points are present in the bin.

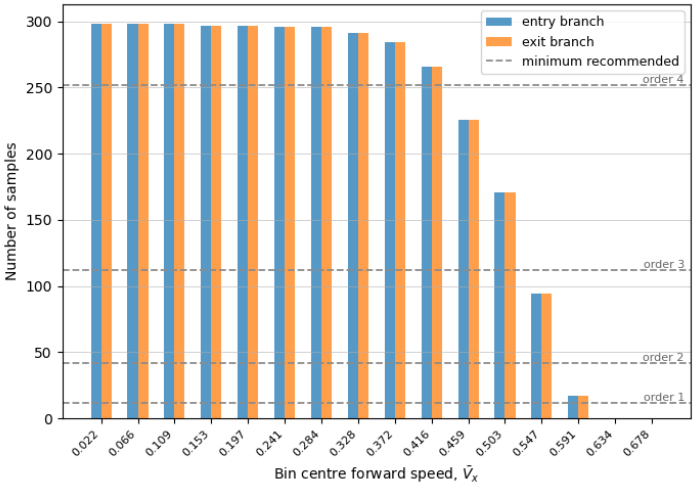


Figure 5.9: Number of valid samples per bin

Figure 5.8a shows mainly linear relations, but Figure 5.8b shows clear non-linear relations. The data is now fit to a second order polynomial (Figure 5.10). Especially Δ_{ring} and $\bar{V}_{peak}$ show inter-parameter effects, seen by the fact that a second-order polynomial allows for a better fit to the data.

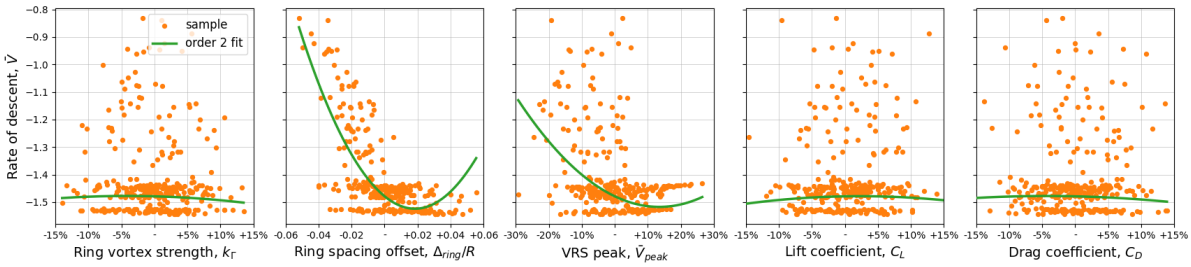
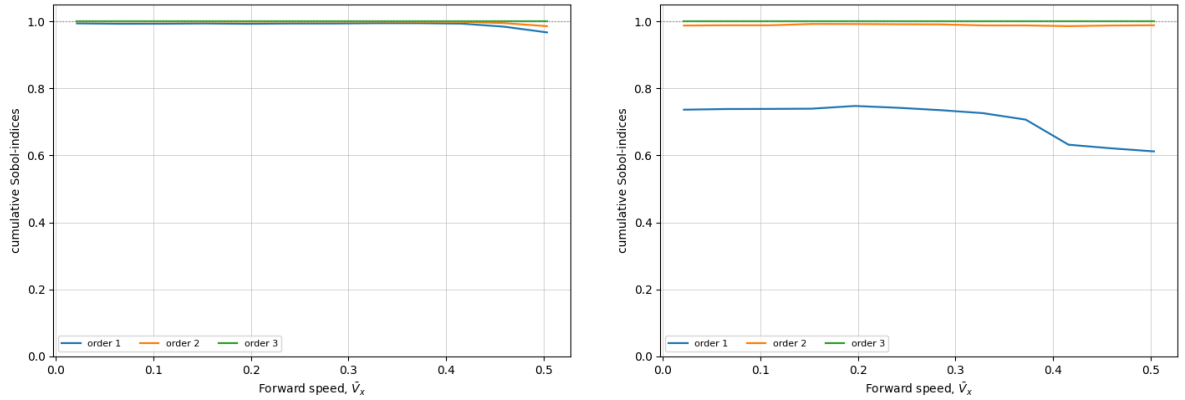


Figure 5.10: Sample scatter with first order polynomial fit

The fitting of curves to the data determines the Sobol-indices, a nondimensional number closely related

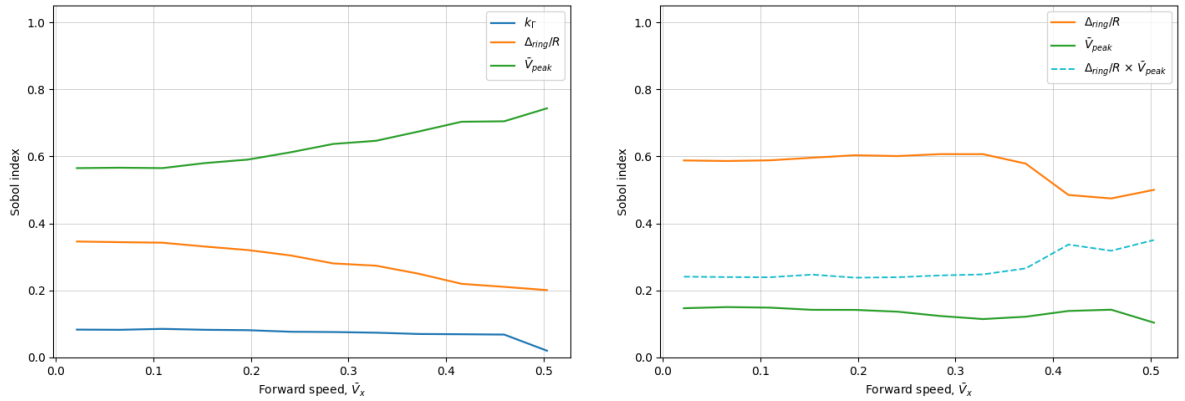
to the coefficients of the fit polynomials (Sobol' 1993). The sum of these Sobol-indices is one if the total variance of the system is fully expressed by the chosen order. Figure 5.11a and Figure 5.11b show the sum of the Sobol-indices for the entry and exit respectively of VRS for a PCE with order one, two and three. Though a first order fit does not show satisfactory results for the exit points, the second order fit captures the full variance, with the third order fit showing little improvement. A second order fit is chosen, as first order will only fully capture the results of the VRS entry and not the exit.



(a) VRS entry **(b)** VRS exit

Figure 5.11: Cumulative Sobol indices

Figure 5.12a and Figure 5.12b show the first and second order Sobol-indices for the entry and exit bounds of VRS. The Sobol-indices of C_L and C_D are excluded from the figure for clarity, as they are (extremely close to) zero. Likewise, k_Γ is filtered out for the exit points and second order Sobol-indices corresponding to combinations of parameters that are essentially zero, are also excluded. For the entry bound of VRS, k_Γ, Δ_{ring}, and $\bar{V}_{peak}$ show to be the most influential parameters. For the exit bound, k_Γ shows to be no longer influential. Instead, the combination of Δ_{ring} and $\bar{V}_{peak}$ is of significance, justifying the use of a second order PCE. This combination is of significant as the ring spacing offset essentially 'breaks the simulation free' from the prescribed peak ($\bar{V}_{peak} = -1.5$), which also explains why the entry bound is not majorly influenced by this combination.



(a) VRS entry **(b)** VRS exit

Figure 5.12: Sobol indices per uncertainty parameter

Figure 5.13 shows the median and 95% certainty bound of VRS using the sampling-based method with LHS and a second order PCE. The polynomials of this PCE are fit to the same 300 samples of the LHS.

PCE shows limited accuracy for both the entry, exit and last $\bar{V}_x$ points. Especially at higher forward speeds, the PCE and LHS results diverge. This divergence stems from two causes. First, for more extreme combinations of the uncertain parameters, RVM occasionally predicts that VRS does not occur at all, such that samples become scarce precisely at these extremes. The fitted polynomial predicts a VRS bound there regardless; a fundamental incompatability between this implementation of RVM and PCE. Second, the relation between the uncertainty parameters and the VRS bounds is not smooth, showing a fluctuation that the smooth polynomial does not capture. Both causes are examined further in Appendix D.

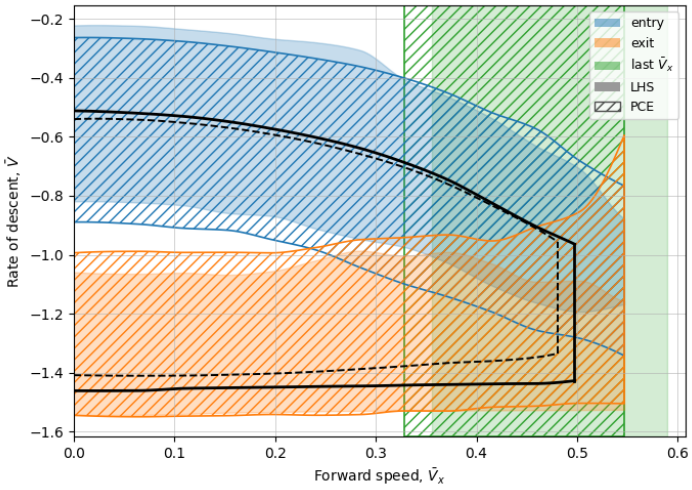


Figure 5.13: Comparison of LHS and PCE 95% certainty band

PCE is deemed incompatible with the implementation of RVM in this thesis. Nevertheless, the uncertainty analysis (specifically the results using LHS) demonstrates that the deterministic trends identified in chapter 4 remain robust. The uncertainty primarily affects the exact position of the VRS boundary rather than the qualitative aerodynamic behavior.

6

Conclusions

The aim of this thesis was to investigate whether a low fidelity model, namely the ring vortex model (RVM), can be used to model the vortex ring state (VRS) for a tandem-rotor helicopter, specifically the CH-47 Chinook. Furthermore, the uncertainty of the VRS bound for both a single rotor and the Chinook was quantified using sampling-based and surrogate-based uncertainty quantification (UQ). The proposed methodology was subsequently evaluated through deterministic simulations and UQ, both compared to experimental flight test data.

Sub-question 1

How can a low fidelity rotor wake model, specifically RVM, be used to predict VRS boundaries for a single rotor?

The RVM model showed a VRS bound for a single rotor that was compared to experimental flight test data. The entry conditions for VRS were found to be in agreement with experimental data until $\bar{V}_x = 0.2$. The exit out of VRS was predicted at higher rates of descent than experimental data suggests for the ONERA flight-test data. This was attributed to a key assumption of RVM; the 'peak' of VRS occurring at a specific rate of descent, $\bar{V}_{peak} = -1.5$. Experimental flight test data from EASA showed to be in agreement for both VRS entry and exit. For forward speeds, key limitations of RVM resulted in a poorer match with experimental data. The results demonstrated that a low-fidelity model can accurately predict VRS entry for axial descent, although its predictive capability decreases for forward speeds over $\bar{V}_x = 0.2$. The conclusion on the applicability to the VRS exit depends on which experimental data the results are compared to.

Sub-question 2

How does rotor-rotor interference influence the predicted VRS boundary in a tandem-rotor configuration like the Chinook?

RVM was expanded for a multi-rotor application, specifically a tandem-rotor, including partly overlapping and intermeshing rotors. This had not been done before. The simulation results showed that rotor-rotor interference fundamentally changes the VRS bounds of each rotor, compared to an identical isolated single rotor. The effects of rotor-rotor interference were most visible at forwards speed higher than $\bar{V}_x = 0.5$ as the wake of the front rotor moved to the aft rotor. Due to the rotor-rotor interference, the front rotor encountered VRS at a higher rate of descent, saw an earlier exit, and VRS ceased to exist at a lower forward speed compared to the aft rotor. The aft rotor showed the opposite behavior, being more prone to VRS. This could result in a dangerous uncommanded pitching tendency for the tandem-rotor configuration. Unfortunately, no data is available to validate these findings for the Chinook.

Sub-questions 3

Which model parameters affect the uncertainty of the predicted VRS boundaries the most?

Key parameters in the model were varied to determine the influence of uncertainty parameters on the VRS bounds. The aerodynamic coefficients C_L and C_D of the blade profile showed no effect on the bounds of VRS, and neither did the mutual inflow k_{mi}. The strength of the vortex rings k_Γ, their normalized position Δ_{ring}/R, the rate of descent at which VRS is at its 'peak' $\bar{V}_{peak}$, and the combination of Δ_{ring}/R and $\bar{V}_{peak}$ showed a significant effect. As an example, the predicted entry into VRS in axial descent for the single rotor had a 95% confidence band between $\bar{V} = -0.25$ and $\bar{V} = -0.8$. For low forward speeds, experimental data (only available for the single rotor) corresponded well to the 95% confidence band, although not enough samples were present in the experimental data to quantify this. Experimental data, especially from ONERA, corresponded better to this 95% confidence band of the VRS bound for the VRS exit than to the singular deterministic bound. Higher forward speeds ($\bar{V}_x > 0.3$) again introduced poorer correlation to the experimental data. For the tandem-rotors, the same conclusions are valid, with the addition of the mutual interference factor k_{mi} having a negligible effect. The model parameters relating to aerodynamic interference (k_Γ, Δ_{ring}/R, $\bar{V}_{peak}$), excluding the mutual inflow for the tandem-rotor, were thus the most influential.

Sub-question 4

Is the uncertainty of the VRS boundary larger at specific (ranges of) forward speeds?

Simulation results showed that the uncertainty for single rotors was fairly constant over the full range of forward speeds. For the multi-rotor, different forward speeds showed different dominant interference effects, and the uncertainty changed accordingly. For the front rotor, the uncertainty grew with forward speed, especially for $\bar{V}_x > 0.2$. For the aft rotor, the uncertainty of the exit bound decreased after $\bar{V}_x = 0.4$, while the entry bound showed a larger uncertainty after $\bar{V}_x = 0.5$. This reflects the transition between dominating interference mechanisms. Overall, the single rotor showed more uncertainty, which is attributed to the mutual inflow of the tandem-rotor being an influential mechanism while carrying less uncertainty.

Sub-question 5

Can PCE, a potentially more computationally efficient method used for UQ, show adequate accuracy compared to LHS when applied to RVM?

Polynomial chaos expansion (PCE) was concluded to be incompatible with this implementation of RVM, because the non-smooth model responses were not approximated to a satisfactory level by polynomials, which was specific to this model. The extreme combinations of uncertainty parameters predicting VRS to not occur at all, while PCE places samples at these extremes regardless, could be a more broad issue that makes PCE unfit for VRS models in general.

Main research question

Can VRS boundaries for single- and tandem-rotor configurations be accurately predicted using RVM, and how do model uncertainties affect these predicted boundaries?

The results from this thesis show that RVM can be used to model VRS boundaries for single rotors. However, only the VRS entry bounds at lower forward speeds correlated to the experimental data. For the tandem-rotor configuration, results aligned with expectations. The tandem-rotor helicopter, especially its aft rotor, was predicted to be more prone to VRS. The uncertainty of the single rotor VRS bound was significant and showed good alignment with experimental data, such that the VRS exit as modeled aligned with experimental data. For the tandem-rotor, the uncertainty was generally smaller and varying due to different interference mechanisms dominating at different forward speeds. The findings on the tandem-rotors could not be validated due to the lack of experimental data.

Overall, this research demonstrated that a computationally efficient RVM-based methodology can successfully predict VRS boundaries and identify the dominant aerodynamic mechanisms governing tandem-rotor interference. Although quantitative accuracy decreased for the VRS exit and at higher forward speeds, the model captured the primary trends relevant for engineering analysis and uncertainty quantification.

7

Recommendations

This research demonstrated that a low-fidelity model can successfully predict the principal characteristics of VRS and quantify the associated uncertainty for single- and tandem-rotor configurations. The results also identified several limitations of the methodology and experimental flight test data that define the most relevant directions for future research regarding VRS boundaries and their uncertainty.

- The deterministic and uncertainty analyses indicated that the primary limitation of the methodology lies in the prescribed wake representation, which is not easily altered. While the RVM provided sufficient accuracy for engineering analyses at modest computational cost, mid-fidelity wake models are expected to improve predictions in forward flight and partially overlapping tandem-rotor configurations. Such models would also reduce uncertainties inherent to the prescribed wake representation, particularly those associated with vortex ring strength and geometry. However, this improvement comes at a higher computational cost, which may reduce the feasibility of large-scale uncertainty quantification. Furthermore, new uncertainties could be introduced.
- The implementation of the RVM should be validated against dedicated experimental flight test data or data from mid- or high-fidelity models for tandem-rotor configurations. Additional single-rotor data would also improve confidence in the model by extending the currently available validation dataset.
- The assumption that both rotor wakes remain independent throughout the computation should be investigated. For partially overlapping and intermeshing rotors, it is conceivable that the interacting tip vortices merge into a single coherent wake structure rather than two independent wakes. Mid- or high-fidelity simulations or experimental measurements are required to determine whether this behavior occurs and whether the current RVM representation remains valid.
- The mutual inflow model is based on several simplifying assumptions and should therefore be validated, particularly within the VRS regime. Alternatively, a different inflow model that computes the local inflow based on the locally produced thrust can be implemented. An example is BET coupled with a momentum theory on a more local level, or one of the more refined inflow models like Peters-He (section 2.4).
- The present model assumes symmetric rotor torque for the Chinook. Any persistent torque imbalance around the yaw-axis of the Chinook would require differential lateral cyclic as it has no tail rotor like a conventional helicopter, altering both the orientation and trajectory of the vortex wake. Including this effect may therefore improve the predicted interaction between both rotors.
- The non-smooth response of this implementation of RVM currently limits the effectiveness of a polynomial surrogate method; PCE. Future work should therefore focus on reducing these numerical discontinuities. It is also to be investigated if PCE is applicable to other VRS models, or if it is not applicable to VRS modeling in general.

References

AeroDynamix (2012). *Wing Tip Vortices 4x High Speed Video*. YouTube video. URL: https://www.youtube.com/watch?v=lslarZiRJhg (visited on 01/22/2026).

Ahlin, Gary A. and Richard E. Brown (2005). "Investigating the Physics of Rotor Vortex Ring State Using the Vorticity Transport Model". In: *Proceedings of the 31st European Rotorcraft Forum*.

— (2009). "Wake Structure and Kinematics in the Vortex Ring State". In: *Journal of the American Helicopter Society*.

Alvarez, Eduardo J. (2022). "Reformulated Vortex Particle Method and Meshless Large Eddy Simulation of Multirotor Aircraft". PhD thesis. Provo, UT, USA: Brigham Young University.

Anusonti-Inthra, Phuriwat et al. (2019). "Sensitivity Analysis and Uncertainty Quantification of a Coaxial Rotor System". In: *AIAA Aviation 2019 Forum*. AIAA 2019-3476. AIAA Paper 2019-3476. Dallas, TX, USA: American Institute of Aeronautics and Astronautics. DOI: 10.2514/6.2019-3476.

Bagai, Ashish and J. Gordon Leishman (1996). "Free-Wake Analysis of Tandem, Tilt-Rotor and Coaxial Rotor Configurations". In: *Journal of the American Helicopter Society* 41.3, pp. 196–207. DOI: 10.4050/JAHS.41.196.

Basset, Pierre-Marie et al. (2008). "Prediction of Vortex Ring State Boundary of a Helicopter in Descending Flight by Simulation". In: *Journal of the American Helicopter Society* 53.2, pp. 139–151.

Benoit, Bernard et al. (2000). "HOST, a General Helicopter Simulation Tool for Germany and France". In: *Proceedings of the 56th Annual Forum of the American Helicopter Society*.

Betoney, Christopher, Basil Celi, and J. Gordon Leishman (2009). "Development of a Free-Vortex Wake Model in State-Space Form". In: *Proceedings of the 35th European Rotorcraft Forum*.

Binet, Laurent and Pierre-Marie Basset (2022). *Helicopter Vortex Ring State Experimental Research*. Tech. rep. VRS D-1.1. Research Project EASA.2022.C11. European Union Aviation Safety Agency.

— (Mar. 26, 2025). *Helicopter Vortex Ring State Experimental Research: D-4.3 Final Report*. Tech. rep. EASA.2022.C11. European Union Aviation Safety Agency. URL: https://www.easa.europa.eu/en/research-projects/vrs-helicopter-vortex-ring-state-experimental-research (visited on 07/10/2026).

Bolkcom, Christopher (Jan. 7, 2005). *V-22 Osprey Tilt-Rotor Aircraft*. CRS Report RL31384. Washington, D.C.: Congressional Research Service. 21 pp. URL: https://digital.library.unt.edu/ark:/67531/metacrs6340/ (visited on 06/18/2026).

Brand, Albert et al. (2007). "The Nature of Vortex Ring State". In: *Proceedings of the American Helicopter Society 63rd Annual Forum*.

Brent, Richard P. (1973). *Algorithms for Minimization without Derivatives*. Englewood Cliffs, NJ: Prentice-Hall. ISBN: 0-13-022335-2.

Brotherhood, P. (1949). *Flow Through a Helicopter Rotor in Vertical Descent*. Tech. rep. Aeronautical Research Council.

Brown, Richard E. (2000). "Rotor Wake Modeling for Flight Dynamic Simulation of Helicopters". In: *AIAA Journal*.

— (2024). "Vortex Ring State and Related Aerodynamic Phenomena in Multi-Rotor Aircraft". In: *Proceedings of the 50th European Rotorcraft Forum*. Paper 129. Marseille, France.

Brown, Richard E. and Andrew J. Line (2005). "Efficient High-Resolution Wake Modeling Using the Vorticity Transport Equation". In: *AIAA Journal*.

Castellin, C. (Sept. 2005). "Isolated Rotor in Vortex Ring State Aerodynamics Using CFD: An Investigation of the Wind Tunnel Effect on Vortex Ring State Aerodynamics". In: *Proceedings of the 31st European Rotorcraft Forum*. Florence, Italy.

Castles, Walter and Robert B. Gray (1951). *Empirical Relation Between Induced Velocity, Thrust, and Rate of Descent of a Helicopter Rotor*. ARC Report. United Kingdom Aeronautical Research Council.

Castles, Walter Jr. and Jacob Henri De Leeuw (1953). *The Normal Component of the Induced Velocity in the Vicinity of a Lifting Rotor and Some Examples of Its Application*. Technical Note NACA TN 2912.

National Advisory Committee for Aeronautics (NACA), p. 38. URL: https://ntrs.nasa.gov/api/citations/19930090980/downloads/19930090980.pdf.

Chae, Seokbong, Seungcheol Lee, and Jooha Kim (2022). "Effects of rotor–rotor interaction on the wake characteristics of twin rotors in axial descent". In: *Journal of Fluid Mechanics* 952, A31. DOI: 10.1017/jfm.2022.913.

Chen, Chang (2006). "Development of a Simplified Inflow Model for a Helicopter Rotor in Descent Flight". PhD thesis. Georgia Institute of Technology.

Chen, Chang and J. V. R. Prasad (2005). "A Simplified Inflow Model of a Helicopter Rotor in Forward Descent". In: *Proceedings of the 43rd AIAA Aerospace Sciences Meeting and Exhibit*.

Chen, Po-Wei et al. (May 13, 2019). "Extraction of Dynamic Inflow Models for Coaxial and Tandem Rotors from CFD Simulations". In: *Proceedings of the Vertical Flight Society 75th Annual Forum & Technology Display*. F-0075-2019-14509. Philadelphia, PA, USA: The Vertical Flight Society. DOI: 10.4050/F-0075-2019-14509. URL: https://ntrs.nasa.gov/api/citations/20190027651/downloads/20190027651.pdf (visited on 05/08/2026).

Choi, Haryun et al. (Jan. 6–10, 2025). "Aerodynamic Interference Analysis for a Coaxial Rotor in Forward Flight Using the Dynamic Vortex Tube Method". In: *AIAA Scitech 2025 Forum*. AIAA 2025-0243. Orlando, FL, USA: American Institute of Aeronautics and Astronautics. DOI: 10.2514/6.2025-0243.

Drees, J. M. (1949). *A Theory of Airflow Through Rotors and its Application to Some Helicopter Problems*. Report TR 18. Amsterdam, The Netherlands: National Aeronautical Research Institute.

Drela, Mark (1989). "XFOIL: An Analysis and Design System for Low Reynolds Number Airfoils". In: *Low Reynolds Number Aerodynamics*. Ed. by Thomas J. Mueller. Vol. 54. Lecture Notes in Engineering. Berlin, Heidelberg: Springer, pp. 1–12. DOI: 10.1007/978-3-642-84010-4_1.

Dutch Safety Board (May 2021). *Crash NH90 Helicopter, Aruba, 19 July 2020: Findings Initial Investigation*. The Hague: Dutch Safety Board. URL: https://onderzoeksraad.nl/wp-content/uploads/2023/11/crash_nh90_helicopter_aruba_findings_initial_investigation.pdf (visited on 08/05/2026).

Dziubinski, Adam and Wienczyslaw Stalewski (2007). "Vortex Ring State Simulation Using Actuator Disc". In: *Proceedings of the 21st European Conference on Modelling and Simulation*. Institute of Aviation, Warsaw. Prague, Czech Republic: European Council for Modelling and Simulation. URL: https://www.scs-europe.net/conf/ecms2007/ecms2007-cd/ecms2007/ecms2007%20pdf/ese_0121.pdf (visited on 06/23/2026).

Fletcher, Timothy M. and Richard E. Brown (2006). "Main Rotor–Tail Rotor Wake Interaction and Its Implications for Helicopter Directional Control". In: *Proceedings of the 32nd European Rotorcraft Forum*.

Froude, Robert Edmund (1889). "On the Part Played in Propulsion by Differences of Fluid Pressure". In: *Transactions of the Institution of Naval Architects* 30, pp. 390–423.

Glauert, Hermann (1926). *The Elements of Aerofoil and Airscrew Theory*. Cambridge University Press.

Hafner, Raoul (1948). "Rotor Systems and Control Problems in the Helicopter". In: *Proceedings of the First Anglo-American Aeronautical Conference*. Presented September 1947. London: Royal Aeronautical Society.

Hahn, Cortney J. et al. (2025). "Characterizing Vortex Ring State During UAV Landing on a Ground Vehicle Using CFD". In: *AIAA SciTech 2025 Forum*.

Hayami, Kaito et al. (2020). "Numerical Investigation of Aerodynamic Interference on Coaxial Rotor". In: *AIAA Scitech 2020 Forum*. AIAA 2020-0306. American Institute of Aeronautics and Astronautics. DOI: 10.2514/6.2020-0306.

He, Chengjian, C. S. Lee, and Weibin Chen (1999). "Technical Note: Finite State Induced Flow Model in Vortex Ring State". In: *proceedings of the American Helicopter Society 55th Annual Forum*.

Hoinville, Eric and Thomas Renaud (May 2007). "CFD Simulation of Helicopter Rotor in the Vortex Ring State Regime". In: *Proceedings of the 63rd Annual Forum of the American Helicopter Society*. Virginia Beach, VA.

Hosder, Serhat, Robert W. Walters, and Michael Balch (Apr. 2007). "Efficient Sampling for Non-Intrusive Polynomial Chaos Applications with Multiple Input Uncertain Variables". In: *9th AIAA Non-Deterministic Approaches Conference*. AIAA Paper AIAA 2007-1939. Honolulu, HI, USA. DOI: 10.2514/6.2007-1939.

Hsieh, Mong-che A. and David A. Peters (2005). "Convergence and Conditioning of Dynamic Wake Models for Flight Dynamics". In: *Proceedings of the 31st European Rotorcraft Forum*. Florence, Italy, pp. 1016–1027. URL: https://dspace-erf.nlr.nl/server/api/core/bitstreams/6c5001a9-c729-43e4-a4f1-54f6754a83ed/content (visited on 07/10/2026).

Jayaraman, B. et al. (2022). "Uncertainty Quantification Approach for Rotorcraft Simulations". In: *Proceedings of the Vertical Flight Society 78th Annual Forum & Technology Display*. F-0078-2022-1239.

Jimenez, Jérémy et al. (2001). "Induced Velocity Model in Steep Descent and Vortex-Ring State Prediction". In: *Proceedings of the 27th European Rotorcraft Forum*.

Johnson, Wayne (2005). *Model for Vortex Ring State Influence on Rotorcraft Flight Dynamics*. Tech. rep. NASA Ames Research Center.

Khurana, Manas, Itham Salah El Din, and Hyeonsoo Yeo (2023). "Uncertainty Quantification of the ONERA 7A Rotor Performance and Loads Using Comprehensive Analysis". In: *Journal of Aircraft* 60.4, pp. 1–19. DOI: 10.2514/1.C036860.

Kim, Hyo Wan et al. (2009). "Interactional Aerodynamics and Acoustics of a Hingeless Coaxial Helicopter with an Auxiliary Propeller in Forward Flight". In: *The Aeronautical Journal*.

Kinzel, Michael P. et al. (Jan. 2019). "An Investigation of the Behavior of a Coaxial Rotor in Descent and Ground Effect". In: *AIAA Scitech 2019 Forum*. AIAA 2019-1098. San Diego, CA, USA. DOI: 10.2514/6.2019-1098.

Leishman, J. Gordon and Ashish Bagai (Oct. 1994). "Free-Wake Analysis of Twin-Rotor Systems". In: *Proceedings of the 20th European Rotorcraft Forum*. Amsterdam, The Netherlands.

Leishman, J. Gordon, Mahendra J. Bhagwat, and Shreyas Ananthan (2002). "Free-Vortex Wake Predictions of the Vortex Ring State for Single-Rotor and Multi-Rotor Configurations". In: *Proceedings of the 58th Annual Forum of the American Helicopter Society*. Montréal, Canada.

— (Apr. 2004). "The Vortex Ring State as a Spatially and Temporally Developing Wake Instability". In: *Journal of the American Helicopter Society* 49.2, pp. 160–175. DOI: 10.4050/JAHS.49.160.

Lewis, James, Andrew J. Lofthouse, and Ashish Bagai (2023). "CFD Study of a Counter-Rotating Propeller eVTOL Concept". In: *AIAA SciTech 2023 Forum*.

Lock, C. N. H., H. Bateman, and H. C. H. Townend (1926). *An Extension of the Vortex Theory of Airscrews with Applications to Airscrews of Small Pitch, Including Experimental Results*. R&M 1014. Aeronautical Research Council.

Makeev, Pavel, Yuri Ignatkin, and Alexander Shomov (2022). "Numerical Study of Coaxial Main Rotor Aerodynamics in Steep Descent". In: *Aerospace* 9.2.

Marshall, M. A. et al. (2024). *Performance of the Dragonfly Lander's Coaxial Rotor in Vortex Ring State*. Tech. rep. NASA Langley Research Center.

McKay, Michael D., Richard J. Beckman, and William J. Conover (1979). "A Comparison of Three Methods for Selecting Values of Input Variables in the Analysis of Output from a Computer Code". In: *Technometrics* 21.2, pp. 239–245. DOI: 10.2307/1268522.

Miller, W. O. and D. B. Bliss (Apr. 1993). "Direct Periodic Solutions of Rotor Free Wake Calculations". In: *Journal of the American Helicopter Society* 38.2, pp. 53–60. DOI: 10.4050/JAHS.38.53.

Mori, Ryuki et al. (2025). "Flow field analysis of Vortex Ring State through descent experiments and simulations with a quadcopter". In: *Journal of Computational Science* 85, 102528. DOI: 10.1016/j.jocs.2025.102528.

Mullen, Paul and Gianni Bernini (Sept. 2016). "Vortex Ring State Prediction and Analysis". In: *Proceedings of the 42nd European Rotorcraft Forum*. Lille, France, pp. 1–36.

Newman, S. J. et al. (2003). "Predicting the Onset of Wake Breakdown for Rotors in Descending Flight". In: *Journal of the American Helicopter Society* 48.1, pp. 28–38. DOI: 10.4050/JAHS.48.28.

Park, S. et al. (2023). "Aerodynamic Interference Analysis for a Nonoverlapping Multirotor UAV Based on Dynamic Vortex Tube". In: *Journal of the American Helicopter Society* 68.4, 042010, pp. 42010–42030. DOI: 10.4050/JAHS.68.042010.

Peters, David A. and Chao He (1995). "Finite-State Induced Flow Models. II—Three-Dimensional Rotor Disk". In: *Journal of Aircraft*.

Peters, David A. and Chengjian He (2006). "Technical Note: Modification of Mass-Flow Parameter to Allow Smooth Transition Between Helicopter and Windmill States". In: *Journal of the American Helicopter Society*.

Piccinini, Riccardo, Matteo Tugnoli, and Alex Zanotti (2021). "Numerical Investigation of the Rotor–Rotor Aerodynamic Interaction for eVTOL Aircraft Configurations". In: *Proceedings of the 47th European Rotorcraft Forum*.

Pitt, D. M. and D. A. Peters (1981). "Theoretical Prediction of Dynamic-Inflow Derivatives". In: *Vertica* 5.1, pp. 21–34.

Prasad, J. V. R. and Chang Chen (2006). "Prediction of Vortex Ring State Using Ring Vortex Model for Single-Rotor and Multi-Rotor Configurations". In: *Proceedings of the AIAA Atmospheric Flight Mechanics Conference and Exhibit*.

Prasad, J. V. R., Morgan Nowak, and Hong Xin (2012). "Finite State Inflow Models for a Coaxial Rotor in Hover". In: *Proceedings of the 38th European Rotorcraft Forum*.

Prasad, J. V. R. et al. (2004). "Simplified Modeling and Non-Linear Analysis of a Helicopter Rotor in Vortex Ring State". In: *Proceedings of the 30th European Rotorcraft Forum*. September 14–16. Marseille, France.

Prouty, Raymond W. (1995). *Helicopter Performance, Stability, and Control*. Malabar, FL: Krieger Publishing Company, p. 95.

QinetiQ (2024). *Vortex Ring State*. Training slides. Climb and Descent, document I3404/GS/03 v3.1. Empire Test Pilots' School.

Radcliff, Eilidh and Marilena D. Pavel (Sept. 9–12, 2025). "Uncertainty Quantification for Rotorcraft Simulation: The Propagation of Modelling Uncertainties to Handling Qualities". In: *Proceedings of the 51st European Rotorcraft Forum*. 51st European Rotorcraft Forum (Venice, Italy). Paper No. 126.

Rankine, William John Macquorn (1865). "On the Mechanical Principles of the Action of Propellers". In: *Transactions of the Institution of Naval Architects* 6, pp. 13–39.

Reeder, John P. and F. B. Gustafson (1949). *On the Flying Qualities of Helicopters*. Technical Note 1799. NACA.

Şenipek, Murat et al. (2023). "System Identification of e-VTOL Rotor in Vortex Ring State by Viscous Vortex Particle Method". In: *Proceedings of the European Rotorcraft Forum*.

Shaler, Kelsey et al. (2020). "Preliminary Introduction of a Free Vortex Wake Method Into OpenFAST". In: *Journal of Physics: Conference Series* 1452.1, 012064. DOI: 10.1088/1742-6596/1452/1/012064.

Sheen, Guanbin et al. (2023). "Modeling of Hovering Intermeshing Rotor Using Blade Element Momentum Theory". In: *Journal of Aircraft* 60.2, pp. 560–575. DOI: 10.2514/1.C036528.

Singh, Puneet and Peretz P. Friedmann (2021). "Dynamic Stall Modeling Using Viscous Vortex Particle Method for Coaxial Rotors". In: *Journal of the American Helicopter Society* 66.1, 012010, pp. 1–16. DOI: 10.4050/JAHS.66.012010.

Siva, C., M. S. Murugan, and Ranjan Ganguli (2011). "Uncertainty Quantification in Helicopter Performance Using Monte Carlo Simulations". In: *Journal of Aircraft* 48.5, pp. 1503–1511. DOI: 10.2514/1.C000288.

Sobol', Ilya M. (1993). "Sensitivity Analysis for Nonlinear Mathematical Models". In: *Mathematical Modelling and Computational Experiment* 1.4. English translation of Sobol' (1990), pp. 407–414.

Sotiropoulos-Georgiopoulos, Eleni et al. (May 16–18, 2023). "A Comparison of Traditional and Vuichard Vortex Ring State Recovery Techniques Using On-Line Simulation". In: *Proceedings of the Vertical Flight Society 79th Annual Forum & Technology Display*. 15-page conference paper. West Palm Beach, FL, USA. DOI: 10.4050/F-0079-2023-18154.

Taghizad, A. et al. (2002). "Experimental and Theoretical Investigation to Develop a Model of Rotor Aerodynamics Adapted to Steep Descents". In: *Proceedings of the 58th Annual Forum of the American Helicopter Society*. Montreal, Canada.

United States Army Warfighting Center (2006). *CH-47D Advanced Flight Control System (AFCS)*. 011-2105-6. Student handout. United States Army Warfighting Center. Fort Rucker, Alabama. URL: https://www.chinook-helicopter.com/standards/Army_D_Model_AQC_Classes/AFCS.pdf (visited on 06/30/2026).

Van Hoydonck, W. R. M., H. Haverdings, and M. D. Pavel (Sept. 22–25, 2009). "A Review of Rotorcraft Wake Modeling Methods for Flight Dynamics Applications". In: *Proceedings of the 35th European Rotorcraft Forum*. Hamburg, Germany: German Society for Aeronautics and Astronautics, pp. 1–28.

Veismann, Marcel et al. (2021). "Axial Descent of Variable-Pitch Multirotor Configurations: An Experimental and Computational Study for Mars Deployment Applications". In: *Vertical Flight Society 77th Annual Forum & Technology Display*.

Vouros, Stavros et al. (2019). "Impact of Wake Modeling Uncertainty on Helicopter Rotor Aeroacoustic Analysis". In: *Proceedings of the 45th European Rotorcraft Forum*. Warsaw, Poland. URL: https://dspace-erf.nlr.nl/bitstreams/7d5bde07-8e79-4b15-8136-82bec110698c/download (visited on 06/25/2026).

Washizu, Kyuichiro et al. (1966). "Experimental Study on the Unsteady Aerodynamics of Model Helicopter Rotors Operating in the Vortex Ring State". In: *Journal of the Japan Society for Aeronautical and Space Sciences*.

Yeates, John E. (1958). *Flight Measurements of the Vibration Experienced by a Tandem Helicopter in Transition, Vortex-Ring State, Landing Approach, and Yawed Flight*. Tech. rep. National Advisory Committee for Aeronautics.

Yuan, Y. et al. (2022). "Aerodynamic Uncertainty Quantification for Tiltrotor Aircraft". In: *Aerospace* 9.5, 271. DOI: 10.3390/aerospace9050271.

Zhao, Guoqing et al. (2025). "Evolution and interaction mechanism of blade tip vortex for coaxial rotors in hover". In: *Aerospace Science and Technology* 165, 110474. ISSN: 1270-9638. DOI: 10.1016/j.ast.2025.110474.

Zhao, Jinggen and Chengjian He (2010). "A Viscous Vortex Particle Model for Rotor Wake and Interference Analysis". In: *Journal of the American Helicopter Society* 55.1, 012007. DOI: 10.4050/JAHS.55.012007.

A

Model Flowcharts

This appendix provides an overview of the model structure used for the single- and multi-rotor configurations. In Figure A.1, the large block (BET) is the main part of the model, in which the inflow model and RVM are used to compute the total inflow. The operating conditions and helicopter geometry are inputs for all these three blocks. From BET, the required collective to keep the rotor thrust trimmed an be determined, after which the VRS boundaries follow from bifurcation. For the tandem-rotor (Figure A.2), the contributions of the second rotor are added. Namely the RVM model for the other rotor, and the mutual inflow.

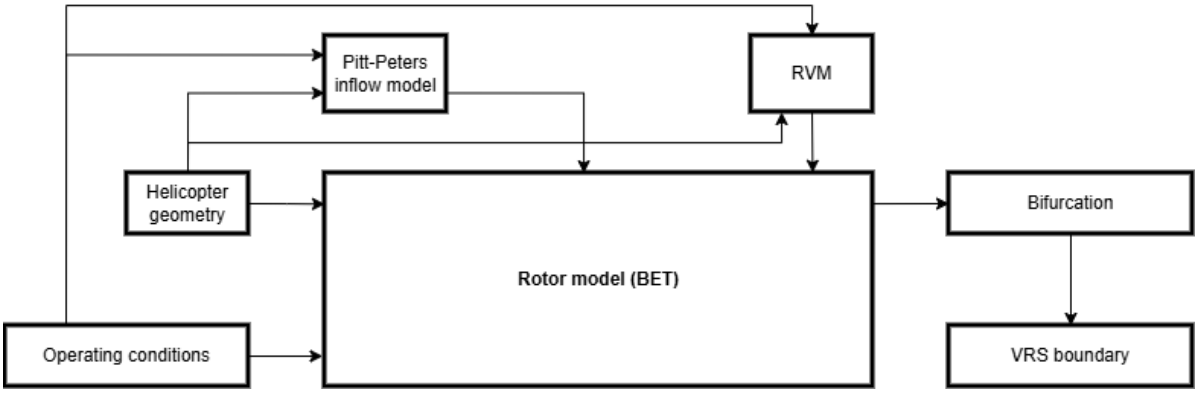


Figure A.1: Flowchart of the single-rotor model

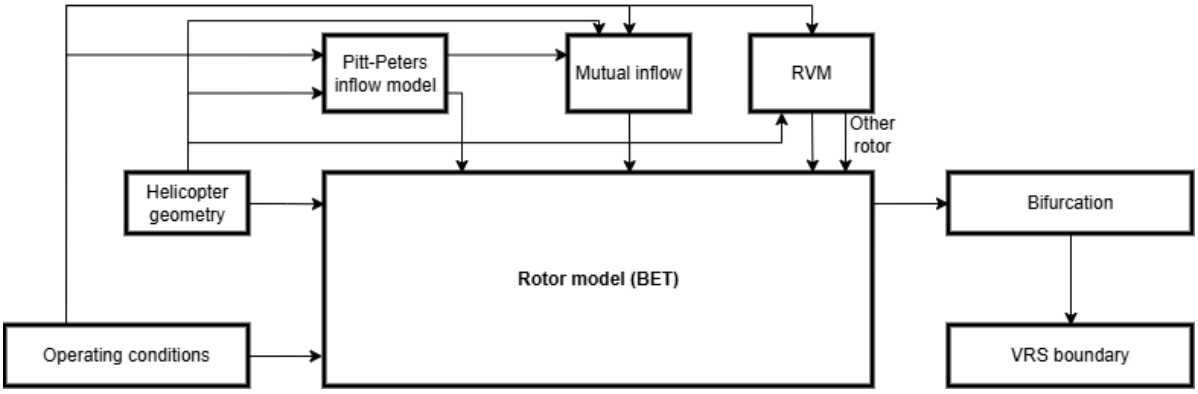


Figure A.2: Flowchart of the multi-rotor model

B

Chinook Model Inputs

The values are gathered from unverified internet sources or internal RNLASF documents and are hence not cited. As the airfoil of the Chinook is not known, the airfoil of the Apache is taken.

Table B.1: Rotor input parameters for the single- and tandem-rotor

Parameter	Symbol	Single-rotor	Tandem-rotor	Unit
Rotor radius	R	7.32		m
Number of blades	N_b	4		–
Rotor speed	Ω	27.0 (257.8)		rad/s (RPM)
Blade chord	c	0.5334		m
Blade airfoil	–	HH02		–
Linear blade twist	θ_{tw}	-12.0		deg
Aircraft weight	W	75 000	150 000	N
Front rotor forward tilt	–	–	7.8	deg
Aft rotor forward tilt	–	–	0.75	deg
Rotor longitudinal separation	–	–	9.49	m
Rotor vertical separation	–	–	1.11	m
Mutual (aft-inflow) interference factor	k_{mi}	–	0.56	–

C

Plots with seperate experimental data

The VRS bound as simulated for a single rotor compared to experimental data of ONERA and EASA (Figure C.1 and Figure C.2, respectively).

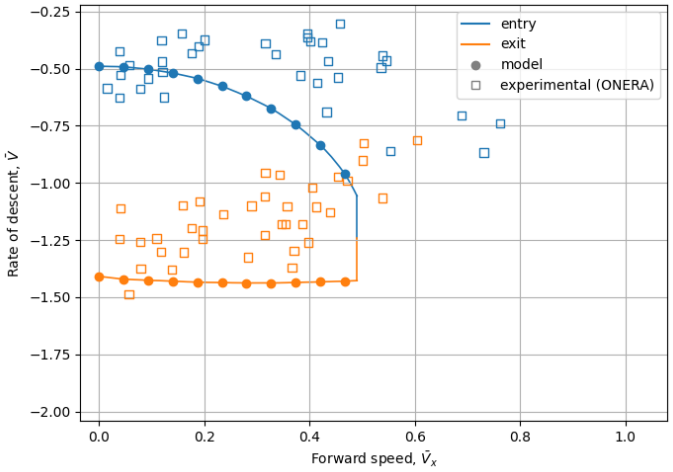


Figure C.1: Predicted VRS entry and exit boundaries compared with ONERA experimental data (Taghizad et al. 2002)

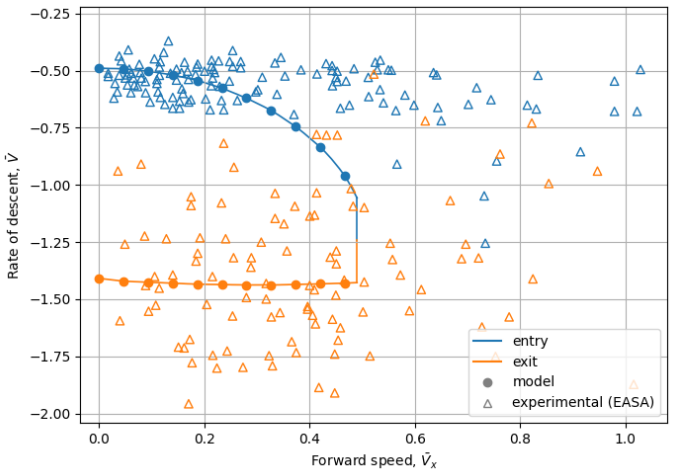


Figure C.2: Predicted VRS entry and exit boundaries compared with EASA experimental data (Binet and Basset 2025)

The 95% certainty band with median for a single rotor compared to experimental data of ONERA and EASA (Figure C.3 and Figure C.4, respectively).

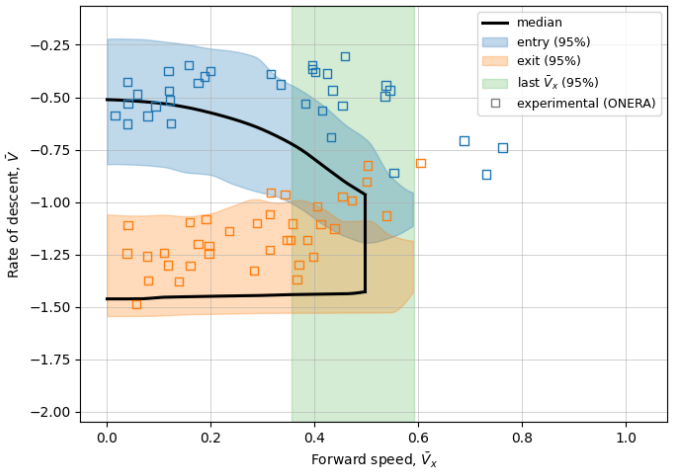


Figure C.3: 95% certainty band of the VRS bound for a single rotor (Taghizad et al. 2002)

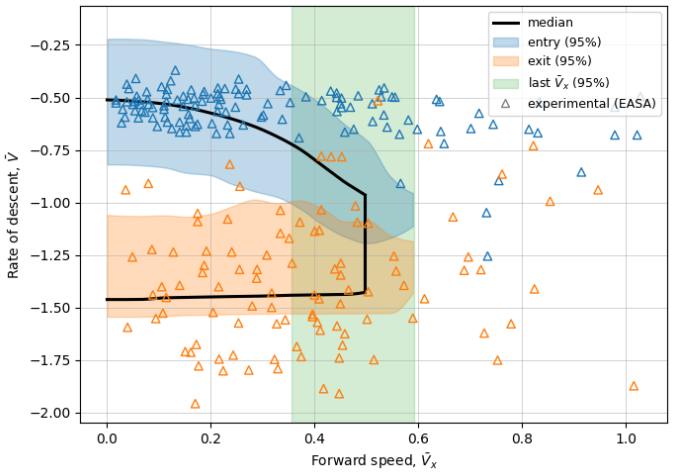


Figure C.4: 95% certainty band of the VRS bound for a single rotor (Binet and Basset 2025)

D

Causes of PCE's limited accuracy

The poor correlation of PCE results compared to the results retrieved using LHS, are of two origins. The first is a fundamental non-compatability between RVM and PCE. When multiple variables hold more extreme values (like the rings being placed far away coupled with an overly large $\bar{V}_{peak}$), VRS is occasionally not predicted to occur at all, or just for lower forward speeds. At these extremes, the amount of samples is thus lacking. Nevertheless, a polynomial is fit, with the surrogate model predicting VRS to occur at these extremes anyway. PCE works better for well-defined 'analytical' relations that are well approximated by a continuous polynomial. This also explains why the results for higher forward speeds ($\bar{V}_x > 0.45$) are so poor. Not only are less samples resulting in valid VRS bounds simply due to VRS ceasing to occur at some forward speed, the samples barely include the aforementioned extreme combinations, such that the fit is even less accurate.

Uniform sampling should theoretically help with scarce sampling at more extreme values, as normal sampling places most samples around the center of the interval. However, this does not mitigate the lack of samples producing a valid VRS bound. Normal sampling resulted in 99.3% of the samples producing a bound around $\bar{V}_x$. In contrast, uniform sampling with more samples at the edges of the intervals, resulted in only 90% of the samples producing a result. This clearly indicates that the lack of samples at the extremes is not a sampling issue.

The second cause of the poor results with PCE is the non-smooth relations between this implementation of RVM and the uncertainty parameters. PCE requires a smooth relation between the uncertain parameter and VRS bounds, as the data is fit with a smooth polynomial. In Figure D.1, $\bar{V}_{peak}$ is varied while the other four uncertain parameters are held constant. The resulting dependency on this uncertainty parameter is not smooth but shows a certain scatter. This scatter of the data is essentially another uncertainty, not stemming from the uncertain parameters previously identified. However, this can also be interpreted as the PCE filtering out uncertainties that are not explicitly modeled.

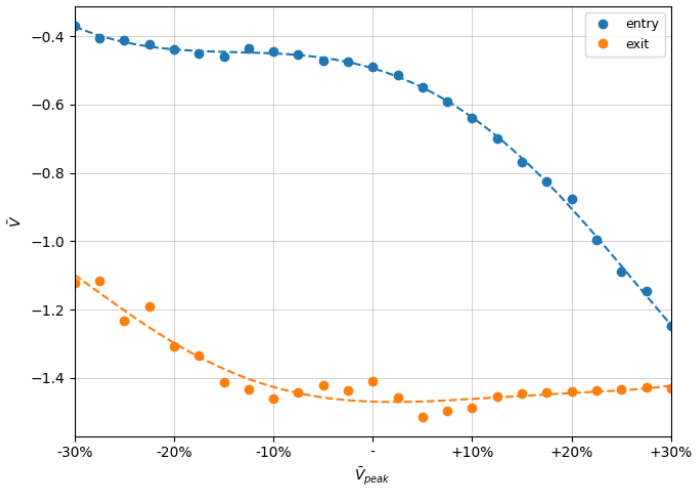


Figure D.1: Relation between VRS bounds and $\bar{V}_{peak}$

Due to these limitations, PCE is considered not compatible with this model for VRS (due to the non-smooth relations), and potentially other VRS models (due to the lack of VRS at extreme combinations of uncertain parameters). For the same reasons, PCE poorly recreates the uncertainty of the tandem-rotor.

E

Vortex-Ring Induced Velocity Formulation

The local induced velocity by a single vortex ring, is taken directly from Castles and De Leeuw (1953). For a point at a nondimensional radial distance x from the ring axis and a nondimensional axial distance z from the ring plane, the following is defined:

$$d_1 = \sqrt{z^2 + (x-1)^2}, \qquad d_2 = \sqrt{z^2 + (x+1)^2}, \qquad \tau = \frac{d_2 - d_1}{d_2 + d_1}, \tag{E.1}$$

The local induced velocity v_i normal to the rotor is:

$$v_i = \frac{\Gamma}{2\pi x R}\,(AB + CDF) \tag{E.2}$$

with

$$A = K(\tau) - E(\tau), \quad B = \frac{x-1}{d_1} + \frac{x+1}{d_2}, \quad C = d_1 + d_2, \quad D = \frac{\tau E(\tau)}{1-\tau^2}, \tag{E.3}$$

$$F = 1 - \frac{(1 + x^2 + z^2) - d_1 d_2}{2x^2} - \frac{(1+x)d_1^2 - (1-x)d_2^2}{2x\, d_1 d_2} \tag{E.4}$$

where $K(\tau)$ and $E(\tau)$ are the complete elliptic integrals of the first and second kind.